ORIGINAL RESEARCH

Hepatocyte-Secreted Autotaxin Exacerbates Nonalcoholic Fatty Liver Disease Through Autocrine Inhibition of the PPARα/FGF21 Axis

Han Qiu,[1,2,*] Erfei Song,[1,2,3,*] Yue Hu,[1,2,*] Tengfei Li,[1,2] Kam Ching Ku,[1,2] Cunchuan Wang,[3] Bernard M. Y. Cheung,[1,2] Lai Yee Cheong,[1,2] Qin Wang,[1,2] Xiaoping Wu,[1,4] Ruby L. C. Hoo,[1,4] Yong Wang,[5,§] and Aimin Xu[1,2,4,§]

[1]State Key Laboratory of Pharmaceutical Biotechnology, The University of Hong Kong, Hong Kong, China; [2]Department of Medicine, The University of Hong Kong, Hong Kong, China; [3]Department of Metabolic and Bariatric Surgery, The First Affiliated Hospital of Jinan University, Guangzhou, China; [4]Department of Pharmacology and Pharmacy, The University of Hong Kong, Hong Kong, China; and [5]Department of General Surgery, The Second Hospital of Anhui Medical University, Hefei, China

SUMMARY

Serum autotaxin levels are closely associated with the histologic severity of nonalcoholic fatty liver disease in obese individuals. Hepatocyte-secreted autotaxin exacerbates nonalcoholic fatty liver disease by autocrine inhibition of peroxisome proliferator-activated receptor α, thereby leading to suppression of hepatic fibroblast growth factor 21 production. Genetic ablation or antibody-mediated neutralization of hepatic autotaxin ameliorates hepatic steatosis, inflammation, and fibrosis in mice.

BACKGROUND & AIMS: The prevalence of nonalcoholic fatty liver disease (NAFLD) has reached epidemic proportions globally as a result of the rapid increase in obesity. However, there is no Food and Drug Administration–approved pharmacotherapy available for NAFLD. This study investigated the role of autotaxin, a secreted enzyme that hydrolyzes lysophosphatidylcholine to produce lysophosphatidic acid (LPA), in the pathogenesis of NAFLD and to explore whether genetic or pharmacologic interventions targeting autotaxin ameliorate NAFLD.

METHODS: The clinical association of autotaxin with the severity of NAFLD was analyzed in 125 liver biopsy-proven NAFLD patients. C57BL/6N mice or fibroblast growth factor 21 (FGF21)-null mice were fed a high-fat diet or a choline-deficient diet to investigate the role of the autotaxin–FGF21 axis in NAFLD development by hepatic knockdown and antibody neutralization. Huh7 cells were used to investigate the autocrine effects of autotaxin.

RESULTS: Serum autotaxin levels were associated positively with histologic scores and NAFLD severity. Hepatocytes, but not adipocytes, were the major contributor to increased circulating autotaxin in both patients and mouse models with NAFLD. In mice, knocking-down hepatic autotaxin or treatment with a neutralizing antibody against autotaxin significantly reduced high-fat diet–induced NAFLD and high fat– and choline-deficient diet–induced nonalcoholic steatohepatitis and fibrosis, accompanied by a marked increase of serum FGF21.

Mechanistically, autotaxin inhibited the transcriptional activity of peroxisome proliferator-activated receptor α through LPA-induced activation of *extracellular* signal-regulated kinas, thereby leading to suppression of hepatic FGF21 production. The therapeutic benefit of anti-autotaxin neutralizing antibody against NAFLD was abrogated in FGF21-null mice.

CONCLUSIONS: Liver-secreted autotaxin acts in an autocrine manner to exacerbate NAFLD through LPA-induced suppression of the peroxisome proliferator-activated receptor α–FGF21 axis and is a promising therapeutic target for NAFLD. *(Cell Mol Gastroenterol Hepatol 2022;14:1003–1023; https://doi.org/10.1016/j.jcmgh.2022.07.012)*

Keywords: Hepatokines; Nonalcoholic Steatohepatitis; Fibroblast Growth Factor; Autocrine Actions; Antibody Therapeutics.

Nonalcoholic fatty liver disease (NAFLD) is the most common form of chronic liver disease that has reached epidemiologic proportions worldwide as a result of the rapid increase in the prevalence of obesity and type 2

diabetes.[1,2] The pathohistologic spectrum of NAFLD ranges from benign steatosis to nonalcoholic steatohepatitis (NASH), the latter of which is characterized by lobular inflammation and ballooning of hepatocytes, with or without perisinusoidal fibrosis. Patients with NAFLD are more susceptible to end-stage liver diseases such as cirrhosis and hepatocellular carcinoma, and are at increased risk for type 2 diabetes, cardiovascular disease, cancer, and overall mortality.[3] NAFLD is expected to become a major indication for liver transplantation in the coming decade.[2,4,5] Despite the rapid increase in the health care burden of NAFLD, there are currently no approved pharmacotherapies for this chronic liver disease

Liver-secreted hepatokines and adipose tissue–secreted adipokines play important roles in controlling metabolic homeostasis, insulin sensitivity, and immunometabolism in the liver.[6] Aberrations in the production and/or function of a large number of hepatokines and adipokines have been implicated in the pathogenesis of NAFLD and its related liver complications.[6,7] A number of hepatokines and adipokines, such as fibroblast growth factor 21 (FGF21) and adiponectin, have been developed as potential therapeutic agents or noninvasive diagnostic biomarkers for NAFLD.[6,8] Autotaxin (ATX), also known as ectonucleotide pyrophosphatase/phosphodiesterase 2, is an adipokine secreted abundantly from mature adipocytes,[9,10] although it also is expressed in many other tissues including the liver. ATX possesses lysophospholipase D (lysoPLD) activity, thereby converting lysophosphatidylcholine to lysophosphatidic acid (LPA),[11] the latter of which is a bioactive lipid that activates multiple cell signaling pathways involved in cell aggregation, proliferation, chemotaxis, and inflammation via binding to its G-protein–coupled receptors.[12,13]

An increasing body of studies has suggested the involvement of the ATX–LPA axis in obesity and its related metabolic complications.[14–17] In adipose tissue, the ATX–LPA axis acts in an autocrine manner to impair insulin actions in white adipocytes, inhibit thermogenesis in brown adipocytes, and in a paracrine manner to promote adipogenesis of preadipocytes.[9] Adipose deletion of ATX has been shown recently to protect against high-fat diet (HFD)-induced obesity, insulin resistance, and glucose intolerance in mice.[18,19] However, another earlier study reported a more obese phenotype of adipose-specific ATX knockout mice.[20] In older human beings with obesity, serum autotaxin correlates positively with adiposity and is an independent predictor of insulin resistance.[21] Aberrant serum autotaxin levels have been observed in patients with severe obesity, viral hepatitis, and fibrosis,[16,22–27] and inhibition of hepatic autotaxin or adipose-derived autotaxin has been reported to alleviate the development of hepatocellular carcinoma[16] or steatosis.[17] However, the pathophysiological role of the ATX–LPA axis in the onset and progression of NAFLD remains to be established.

In this study, we measured the dynamic changes in circulating levels of autotaxin and its hepatic expression in several different mouse models with NAFLD, and explored the relationship of serum autotaxin with histologic severity and progression of NAFLD in liver biopsy–proven patients. Furthermore, we investigated the role of liver-secreted autotaxin in NAFLD development by both knockdown of hepatic autotaxin and treatment with a neutralizing antibody against autotaxin, and delineated the pathogenic mechanism whereby the aberrant ATX–LPA axis exacerbates NAFLD via dysregulation of FGF21.

Results

Serum Autotaxin Levels Are Closely Associated With Abnormal Liver Function and NAFLD Severity in Obese Individuals

To investigate the clinical association of autotaxin with liver function and the severity of NAFLD, we consecutively recruited 151 obese individuals undergoing bariatric surgery. The clinical, biochemical, and histologic characteristics of the 151 obese subjects included in this study are shown in Table 1. The mean ± SD age and body mass index (BMI) of the participants were 30.35 ± 1.35 y and 40.23 ± 1.24 kg/m^2, respectively. Histologic examination of liver biopsy specimens showed that the prevalence of hepatic steatosis (at least 5% of fat within hepatocytes), ballooning, inflammation, and fibrosis occurred in 132 (87.4%), 80 (53.0%), 70 (46.3%), and 38 (25.2%) patients, respectively. A total of 14 (9.3%) patients showed normal liver histology, while 31 (20.5%), 62 (41.1%), and 44 (29.1%) patients were classified into simple steatosis, borderline NASH, and NASH, respectively, according to the fatty liver inhibition of progression algorithm.[28] Consistent with previous reports,[21] serum autotaxin levels in women (508.53 ± 21.58 ng/mL; n = 85) were significantly higher than in men (417.33 ± 22.48 ng/mL; n = 66; $P = .004$, Mann–Whitney U test). Notably, serum autotaxin levels showed significant positive correlations with hepatic fat content (determined by magnetic resonance imaging); serum levels of the liver injury markers aspartate aminotransferase (AST) and alanine aminotransferase (ALT) (Figure 1A–C); severity scores of hepatic steatosis, ballooning, and inflammation grade; as well as histologic progression of NAFLD from normal liver, benign steatosis to NASH. These significances remained even after adjustment for sex, age, and BMI (Table 2). Real-time polymerase chain reaction (PCR) analysis showed a significantly higher protein level of autotaxin in the liver tissue than in subcutaneous and visceral adipose tissues of obese individuals (Figure 1D). Furthermore, there was a strong positive association between serum autotaxin levels and the autotaxin messenger RNA (mRNA) expression in the liver, but not in adipose tissues (Figure 1E). Taken together, these findings suggest that increased serum autotaxin is associated closely with the development of liver dysfunction and NAFLD progression in obese individuals, and the liver is perhaps an important contributor to increased circulating autotaxin.

Liver But Not Adipose Tissue Contributes to Increased Circulating Autotaxin in Mouse Models With NAFLD

To confirm our findings in the earlier-described clinical study, we monitored the dynamic changes of the autotaxin mRNA expression in major organs, serum autotaxin levels,

Table 1. Clinical Characteristics of the Obese Subjects Included in This Study

Parameters	Normal (n = 14)	Steatosis (n = 31)	Borderline NASH (n = 62)	NASH (n = 44)	P value
Age, y	32.61 ± 2.82	31.64 ± 1.36	30.23 ± 0.91	28.90 ±1.14	.303
Sex, male:female	4:10	12:19	29:33	21:23	.000
BMI, kg/m^2	33.38 ± 1.62	39.77 ± 1.61	40.52 ± 0.92	42.34 ± 1.19	.002
Neck circumference, cm	38.43 ± 1.02	42.41 ± 0.77	43.10 ± 0.57	44.19 ± 0.72	.000
Waist circumference, cm	106.36 ± 3.14	124.35 ± 3.15	123.70 ± 1.77	128.44 ± 2.55	.000
Hip circumference, cm	115.05 ± 2.95	125.78 ± 2.93	125.24 ± 1.54	129.94 ± 2.13	.003
C-peptide, ng/mL	2.22 ± 0.23	3.38 ± 0.16	3.79 ± 0.12	4.58 ± 0.23	.000
Glucose, mmol/L	5.27 ± 0.23	6.45 ± 0.58	6.55 ± 0.35	6.82 ± 0.36	.274
HbA1c, %	5.50 ± 0.20	6.02 ± 0.19	6.30 ± 0.19	6.54 ± 0.20	.061
Insulin, mU/L	13.21 ± 1.65	19.91 ± 1.59	22.41 ± 1.55	35.09 ± 4.91	.000
HOMA-IR	3.08 ± 0.42	5.49 ± 0.54	6.63 ± 0.57	11.02 ± 2.15	.003
HOMA-B	1.69 ± 0.17	2.04 ± 0.21	2.16 ± 0.17	2.83 ± 0.26	.012
ALT, U/L	22.86 ± 2.29	49.99 ± 8.22	69.34 ± 6.67	77.15 ± 8.75	.001
AST, U/L	19.73 ± 1.91	30.34 ± 3.60	40.63 ± 3.27	51.98 ± 5.93	.000
Adenosine deaminase, U/L	12.17 ± 0.70	14.02 ± 0.87	15.12 ± 0.52	17.10 ± 0.70	.000
TCHOL, mg/dL	4.82 ± 0.17	4.98 ± 0.18	5.14 ± 0.12	5.17 ± 0.16	.524
HDL-C, mg/dL	1.09 ± 0.05	1.08 ± 0.05	1.02 ± 0.02	0.97 ± 0.23	.114
LDL-C, mg/dL	2.97 ± 0.12	2.95 ± 0.13	3.19 ± 0.09	3.07 ± 0.12	.411
Triglyceride, mg/dL	1.41 ± 0.11	2.77 ± 1.19	2.30 ± 0.20	3.02 ± 0.55	.437
Ferritin, mg/L	88.86 ± 29.29	164.99 ± 29.85	180.97 ± 22.17	202.24 ± 24.91	.069
Total bilirubin, U/L	10.45 ± 1.01	11.98 ± 1.02	13.31 ± 0.79	14.58 ± 0.71	.037
Direct bilirubin, U/L	2.96 ± 0.92	2.37 ± 0.20	3.16 ± 0.22	3.60 ± 0.22	.055
Lipoprotein a, mg/dL	194.12 ± 75.35	188.66 ± 45.74	187.43 ± 29.67	91.05 ± 14.62	.000
Apolipoprotein B, g/L	0.92 ± 0.04	0.98 ± 0.03	1.09 ± 0.23	1.05 ± 0.04	.016
Lactate dehydrogenase, U/L	176.40 ± 10.08	202.93 ± 9.91	212.54 ± 6.10	222.89 ± 9.36	.024

NOTE. Data are expressed as means ± SEM.
HbA1c, glycated hemoglobin (A1c); HDL-C, high-density lipoprotein cholesterol; HOMA-B, HOMA of β-cell function index; HOMA-IR, homeostasis model assessment of insulin resistance; LDL-C, low-density lipoprotein cholesterol; TCHOL, total cholesterol.

as well as lysoPLD activity in HFD-induced obese mice with NAFLD and lean controls for a period of 20 weeks. Serum autotaxin levels and lysoPLD activity showed a progressive increase with the progression of diet-induced obesity (Figure 2A and B), but remained little changed in standard chow diet (STC)-fed lean mice. At 20 weeks after HFD start, serum autotaxin levels and lysoPLD activity in obese mice were 1.65- and 2-fold higher than in lean mice, respectively (Figure 2A and B). In line with previous reports showing autotaxin as an adipokine,[9,18,29] real-time PCR analysis detected highly enriched mRNA expression of autotaxin in several adipose depots, including epididymal white adipose tissue and interscapular brown adipose tissue (Figure 2C). However, the autotaxin mRNA expression in these 2 adipose depots paradoxically were decreased in HFD-induced obese mice compared with that in lean mice, although there was a modest increase of autotaxin gene expression in subcutaneous white adipose tissue of obese mice. In contrast, the autotaxin mRNA expression level in the liver of HFD-induced obese mice was increased significantly by almost 2-fold, whereas its mRNA abundance in other tissues was comparable between obese and lean mice, except for lymph nodes, where autotaxin mRNA expression in obese mice was lower than in lean mice. Further cellular fractionation analysis showed that the autotaxin gene expression in hepatocytes was more than 5-fold higher than in nonparenchymal cells, while obesity-induced up-regulation of the autotaxin gene expression occurred predominantly in hepatocytes, but not in nonparenchymal cells (Figure 2D).

To further dissect the contribution of adipose tissue and liver to circulating autotaxin in mice with NAFLD, we next used adipocyte-specific murine double-minute 2 (MDM2) knockout (KO) mice, which showed complete loss of adipose tissues, severe hyperglycemia, dyslipidemia, and massive fatty liver.[30,31] Surprisingly, the autotaxin mRNA expression in the liver of the lipodystrophic mice was more than 3-fold higher than in wild-type (WT) littermates, accompanied by a significant increase of serum autotaxin (Figure 2E and F). On the other hand, the autotaxin gene expression level in other tissues was comparable between these 2 genotypes of mice (Figure 2F). Taken together, these findings suggest that hepatocytes, but not adipose tissues, are the major
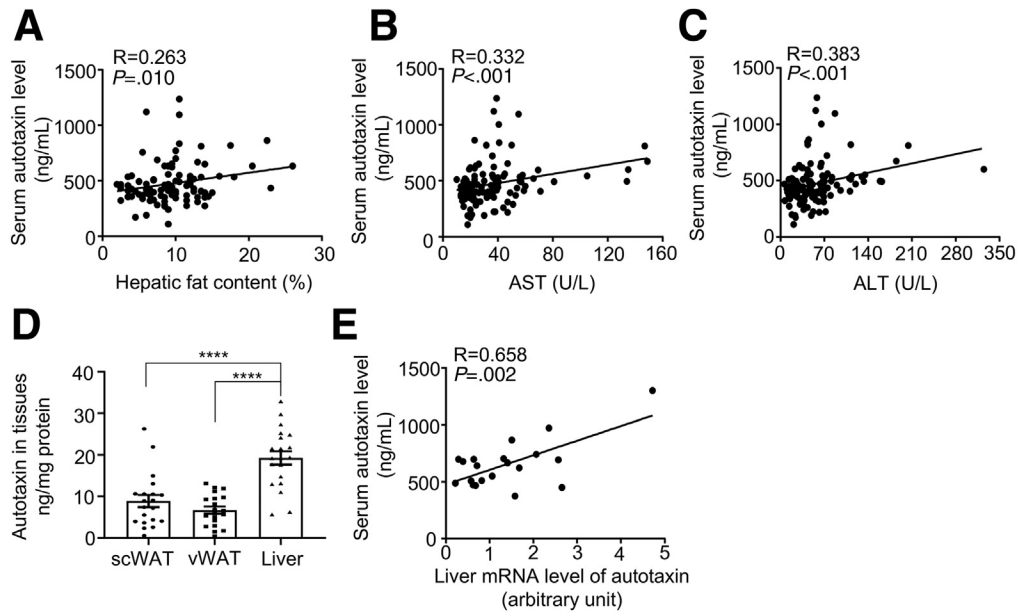
Figure 1. Association of serum autotaxin levels with liver fat contents, liver injury markers, and hepatic autotaxin mRNA expression in obese human subjects. Correlation of serum autotaxin levels with liver fat content determined by (*A*) magnetic resonance imaging (n = 101), (*B*) serum levels of AST (n = 125), and (*C*) ALT (n = 125). (*D*) Protein levels of autotaxin in subcutaneous fat (scWAT), visceral fat (vWAT), and liver in man or woman obese patients (n = 10 each) measured by enzyme-linked immunosorbent assay. The difference was analyzed with 1-way analysis of variance followed by Tukey multiple comparisons. ****$P < .0001$, data are plotted and expressed as means $\pm$ SEM. (*E*) Correlation of hepatic autotaxin mRNA abundance with serum autotaxin levels (n = 20).

production site for increased circulating autotaxin in both dietary obese mice and lipodystrophic mice with NAFLD.

Knock-Down of Hepatic Autotaxin Expression Alleviates NAFLD by Increasing Fatty Acid Oxidation in Obese Mice

Conventional autotaxin KO mice are embryonic lethal owing to the pivotal role of autotaxin in angiogenesis and development.[32] To investigate the role of liver-secreted autotaxin in obesity-induced metabolic complications and fatty liver disease, we used the adeno-associated virus (AAV) 2/8 delivery system to knock-down (KD) hepatic autotaxin in adult mice by intravenous injection of AAV directly to the liver. Compared with the mice injected with AAV expressing scramble control, the mRNA expression of autotaxin in the liver of STC-fed lean mice and HFD-fed obese mice was decreased significantly by 40% and 45%, respectively, after injection of AAV bearing short hairpin RNA (shRNA) specific to the autotaxin (KD) gene for 15 weeks (Figure 3*A*), whereas autotaxin gene expression in adipose tissues remained unchanged (Figure 3*B*). Notably, HFD-induced increases of serum autotaxin levels and lysoPLD activity largely were abrogated by AAV-mediated KD of hepatic autotaxin (Figure 3*C* and *D*), further confirming the liver as a major contributor to increased circulating autotaxin in obesity.

KD of hepatic autotaxin did not exert an obvious effect on body weight, total fat mass, and food intake (Figure 3*E*–*G*), but significantly improved lipid profiles in

Table 2. Association of Serum Autotaxin Levels With Histologic Severity of Biopsy-Confirmed NAFLD (n = 125)

Severity of pathohistology	Pseudo R	P value
Steatosis	0.318	.001**
Inflammation	0.353	.000***
Ballooning	0.297	.003**
Fibrosis	0.657	.252
Histology diagnosis (normal liver, simple steatosis, borderline NASH, and NASH)	0.383	.000***

NOTE. The scores of steatosis (0–3), hepatocellular ballooning (0–2), lobular inflammation (0–3), and fibrosis (0–4) were evaluated according to the NASH Clinical Research Network scoring system. R: Correlation coefficient.
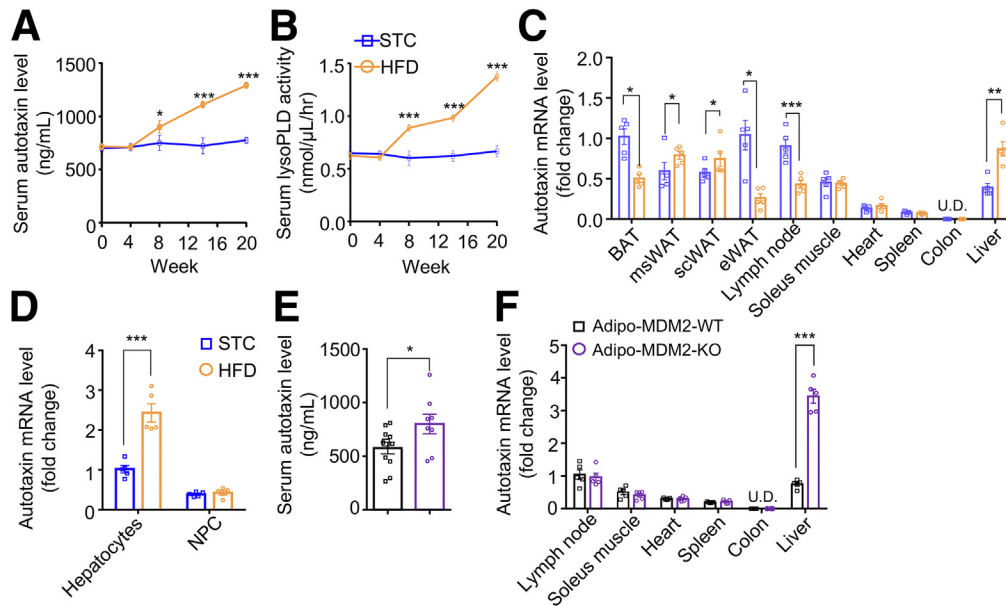**$P < .01$.
***$P < .001$.

Figure 2. Liver is a major contributor to increased circulating autotaxin in mice with NAFLD. (*A–D*) Six-week-old C57BL/ 6N male mice (n = 5) were fed a STC or HFD for 20 weeks and then were killed to collect serum and various tissues for further analysis. Time-dependent changes in (*A*) serum level of autotaxin protein and (*B*) lysoPLD activity. The relative mRNA abundance of (*C*) mouse autotaxin in different tissues (shown as fold change relative to brown adipose tissue [BAT] of the STC group), and in (*D*) different fractions of the liver (shown as fold change relative to hepatocytes of the STC group) determined by real time PCR analysis. *$P < .05$, **$P < .01$, and ***$P < .001$ vs STC group. Data are presented as the means ± SEM. Twelve-week-old male adipocyte-specific MDM2 KO mice and their WT littermates (adipo-MDM2-WT) were killed to collect (*E*) serum and various tissues for measurement of circulating autotaxin (n = 8–12) and (*F*) relative mRNA abundance of autotaxin (n = 5, shown as fold change relative to lymph node of adipo-MDM2-WT group) by enzyme-linked immunosorbent assay and real-time PCR, respectively. (*A–F*) Statistical significance was determined by a 2-tailed Student *t* test. *$P < .05$, and ***$P < .001$ vs the Adipo-MDM2-WT group. Data are presented as the means ± SEM. eWAT, epididymal adipose tissue; msWAT, mesenteric adipose tissue; NPC, nonparenchymal cell.

dietary obese mice, including reductions in serum triglyceride, cholesterol, and free fatty acids (Figure 4*A*). Moreover, hepatic knockdown of autotaxin markedly alleviated HFD-induced increases of liver weight (Figure 4*B*) and hepatic steatosis, as determined by H&E and Oil Red O staining (Figure 4*C*), and biochemical analysis for hepatic triglyceride contents (Figure 4*D*). Accordingly, increased serum levels of ALT and AST, the 2 well-established markers of liver injury, were decreased markedly in obese mice with knockdown of hepatic autotaxin (Figure 4*E*).

Excessive hepatic lipid accumulation often is caused by an imbalance between fatty acid oxidation (FAO) and de novo lipogenesis.[4] We next examined the impact of knockdown of hepatic autotaxin on expression of genes involved in hepatic lipid metabolism and found that several FAO-related genes, including *Cpt1a*, *Mcad/Lcad/Scad*, and *Acox1* were increased greatly in both lean and obese mice with AAV-mediated knockdown of hepatic autotaxin (Figure 4*F*), whereas genes involved in fatty acid synthesis such as *Fasn* and *Scd-1* were not affected. Furthermore, increased hepatic FAO gene expression in the autotaxin knockdown mice was accompanied by a significant increase in FAO activity in the liver, as determined by reduced nicotinamide adenine dinucleotide–dependent production of iodonitrotetrazolium (INT)-formazan (Figure 4*G*). Taken together, these findings suggest that blocking augmented hepatic autotaxin expression is sufficient to counteract obesity-related NAFLD, possibly by increasing FAO.

Treatment With Anti-Autotaxin Neutralizing Antibody Potently Ameliorates Hepatic Steatosis and Increases Hepatic FGF21 in Obese Mice

Given that autotaxin is a secreted enzyme with lysoPLD activity, we generated a neutralizing antibody (IgG) against autotaxin (anti-ATX) and evaluated whether neutralization of secreted autotaxin has therapeutic benefits on obesity-related NAFLD. Ex vivo incubation of serum from obese mice with anti-ATX IgG dose-dependently inhibited the endogenous lysoPLD activity with half maximal inhibitory concentration and maximum inhibitory effects at concentrations of 0.069 and 0.251 umol/L, respectively, whereas nonimmune IgG had no such inhibitory effect (Figure 5*A*). Furthermore, treatment with anti-ATX but not nonimmune IgG blocked the lysoPLD activity of recombinant mouse autotaxin (rmATX) and suppressed the stimulatory effects of rmATX on phosphorylation of *extracellular* signal-regulated kinase (ERK)1/2 in HepG2 hepatocytes in a concentration-dependent manner (Figure 5*B* and *C*). The circulating half-life of anti-ATX IgG in mice was approximately 5 days (Figure 5*D*).
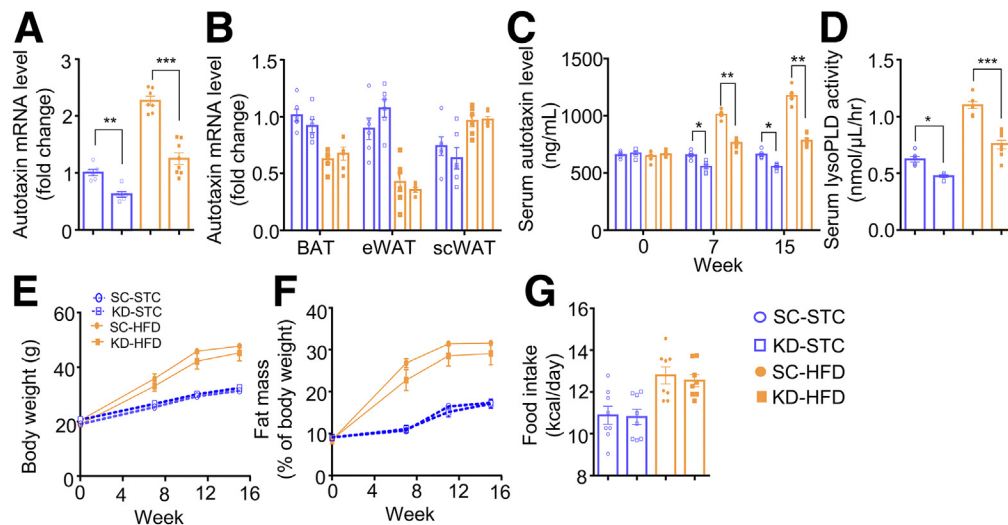
Figure 3. Knockdown of hepatic autotaxin expression decreases obesity-induced increases of circulating autotaxin levels and lysoPLD activity but has no effect on body weight and food intake. Six-week-old C57BL/6N male mice were injected intravenously with 1×10^{11} vector genome of AAV encoding shRNA specific to autotaxin (KD) or scramble control (SC), and then were fed with STC or HFD for 15 weeks. Real-time PCR analysis for mRNA expression levels of autotaxin in (*A*) liver (shown as fold change against the SC-STC group) and in (*B*) different adipose depots (shown as fold change against brown adipose tissue [BAT] of the SC-STC group). (*C*) Serum autotaxin levels measured at different time points after AAV injection. (*D*) Serum lysoPLD activity measured at the 15th week after AAV injection. (*E*) Body weight and (*F*) fat mass measured at the indicated time points; (*G*) average daily food intake shown as kilocalories per day. n = 6–8. (*A–G*) Statistical calculations were performed by 1-way analysis of variance followed by Tukey multiple comparisons using Prism 6. *$P < .05$, **$P < .01$, and ***$P < .001$. Data are presented as the means ± SEM. eWAT, epididymal adipose tissue; scWAT, subcutaneous adipose tissue.

Treatment of mice with anti-ATX IgG for a period of 7 weeks decreased circulating lysoPLD activity (Figure 6*A*) and significantly reduced HFD-induced increase of serum triglycerides, cholesterol, and free fatty acids (FFAs) (Figure 6*B*), although it had no significant effect on body weight, body composition, and food intake (Figure 5*E–G*). In line with the findings in mice with knockdown of hepatic autotaxin, obese mice treated with anti-ATX IgG showed obvious improvements in NAFLD, as evidenced by significant reductions in liver weight (Figure 6*C*), hepatic steatosis (Figure 6*D*), triglyceride accumulation (Figure 6*E*), and serum levels of ALT and AST (Figure 6*F*). These improvements in anti-ATX IgG-treated mice were accompanied by up-regulated expression of hepatic genes involved in FAO (Figure 6*G*), and increased FAO activity in the liver (Figure 6*H*).

Crosstalk between liver-secreted hepatokines and adipose-secreted adipokines play important roles in regulating hepatic lipid metabolism.[6] Therefore, we next examined the effects of anti-ATX IgG on serum levels of a panel of well-established hepatokines and adipokines involved in the pathogenesis of NAFLD.[6] Treatment of mice with anti-ATX IgG had no obvious effects on mRNA expression levels of lipocalin-2, Fgf15, Angptl3/4/6, Fetuin-a, Fgl-1, Dpp4, Fabp4, leptin, and Apelin (Figure 7*A* and *B*), but markedly increased serum levels of FGF21 as well as the hepatic mRNA expression of FGF21 (Figure 7*C* and *D*), a well-known hepatokine with protective effects against NAFLD.[8] Accordingly, serum level of adiponectin, a downstream

effector of FGF21 with anti-steatosis activity,[33] also was increased by anti-ATX IgG (Figure 7*E*). Likewise, significant increases in hepatic FGF21 expression and serum levels of FGF21 and adiponectin also were observed in mice with AAV-mediated knockdown of hepatic autotaxin expression (Figure 7*F–H*).

Autotaxin Inhibits Hepatic FGF21 Production Through LPA-Induced ERK Activation and Peroxisome Proliferator-Activated Receptor α Inhibition

The earlier-described findings suggest that autotaxin may exacerbate NAFLD via inhibition of hepatic FGF21 production. Therefore, we next investigated the direct effects of autotaxin and its enzyme product LPA on FGF21 expression in Huh7 hepatocytes. The *Fgf21* mRNA abundance and FGF21 secretion into conditioned medium were decreased significantly by treatment with recombinant human autotaxin (rhATX), but were obviously increased by incubation with PF8380 (a chemical compound that selectively inhibits the lysoPLD activity of autotaxin to produce LPA[34]) and Ki16425 (a pharmacologic LPA-receptor antagonist[35]) (Figure 7*I* and *J*), suggesting the ATX–LPA axis acts in an autocrine manner to suppress endogenous FGF21 production in hepatocytes. Likewise, treatment of Huh7 hepatocytes with rhATX and LPA dose-dependently inhibited the peroxisome proliferator-activated receptor α (PPARα) agonist fenofibrate-induced Fgf21 mRNA
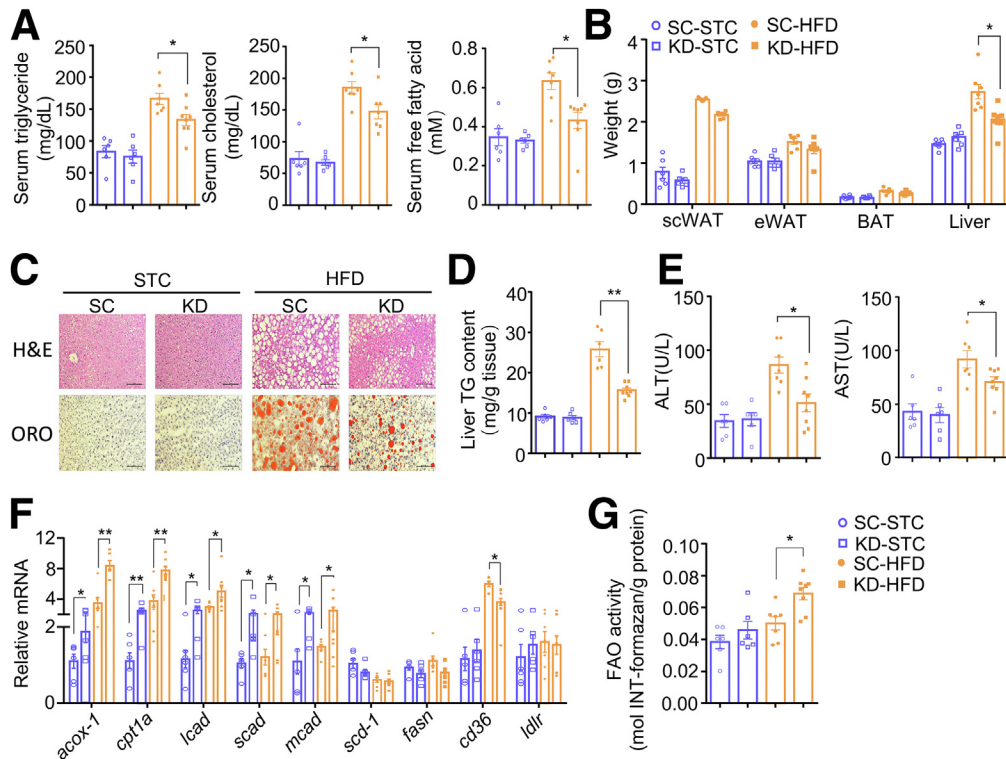
Figure 4. The effect of knockdown of hepatic autotaxin expression on obesity-related NAFLD. Six-week-old C57BL/6N male mice were fed with STC or HFD for 15 weeks after intravenous injection with 1×10^{11} vector genome of AAV encoding shRNA specific to autotaxin (KD) or scramble control (SC). (*A*) Serum lipid profiles including levels of triglycerides, cholesterol, and free fatty acid. (*B*) Wet weight of different organs. (*C*) Representative photos of H&E staining and Oil Red O (ORO) staining of liver sections (200×; *scale bar*: 100 um). (*D*) Hepatic triglyceride (TG) content determined by biochemical analysis. (*E*) Serum levels of ALT and AST. (*F*) Real-time PCR analysis for genes involved in hepatic lipid metabolism. Genes were normalized with β-*actin* and shown as fold change relative to the SC-STC group. (*G*) FAO rate in livers. Oxidation of fatty acid is coupled to reduced nicotinamide adenine dinucleotide–dependent reduction of INT to INT-formazan. FAO activity was shown as the production of INT-formazan (mol) per gram protein. n = 6–8. (*A*, *B*, and *D*–*G*) Statistical calculations were performed by 1-way analysis of variance followed by Tukey multiple comparisons using Prism 6. *$P < .05$, **$P < .01$. Data are presented as the means ± SEM. BAT, brown adipose tissue; eWAT, epididymal adipose tissue; scWAT, subcutaneous adipose tissue.

expression and its protein secretion, whereas such inhibitory effects of endogenous autotaxin were reversed by preincubation with PF8380 and Kil6465 (Figure 7*K* and *L*). Autotaxin-derived LPA exerts its pleiotropic effects by activating several intracellular signaling cascades, especially phosphoinositide 3-kinases/protein kinase B (PI3K/Akt) and mitogen-activated protein kinase/extracellular signal-regulated kinases (MAPK/ERK) pathways.[36] Our results showed that treatment with the selective inhibitor of mitogen-activated protein kinase kinase/extracellular signal-regulated kinases (MEK/ERK, U0126) markedly reversed the inhibitory effect of LPA on fenofibrate-induced FGF21 production, whereas the PI3K inhibitor (wortmannin) had no obvious effect (Figure 7*O*). Given that PPARα is a key regulator for FGF21 gene expression in hepatocytes,[37,38] we next investigated whether LPA suppresses FGF21 production through ERK-mediated inhibition of PPARα. In Huh7 cells transfected with the PPAR response element X3-TK-luc promotor plasmid,[39] LPA treatment significantly decreased fenofibrate-induced transcriptional activity of PPARα as determined by the luciferase reporter analysis, whereas such a suppressive effect of LPA was largely reversed by U0126, but not wortmannin (Figure 7*P*).

Likewise, LPA significantly reduced the expression of another well-known PPARα target gene, *Vlcad*, through ERK activation (Figure 7*O*). In contrast, PPARα mRNA abundance was not affected by either LPA or U0126 (Figure 7*O*).

PPARα activity can be modulated post-translationally by ERK-mediated phosphorylation,[40–42] and 2 ERK phosphorylation sites (S12 and S21) have been identified in mouse PPARα, which are highly conserved between species.[41,42] We next explored the effect of LPA on PPARα phosphorylation at these 2 sites with Western blot. As expected, LPA induced ERK phosphorylation at Ser 21, which was blocked by U0126 (Figure 7*M* and *N*), whereas neither LPA nor U0126 had any effect on phosphorylation at Ser 12. Taken together, these findings suggest that autotaxin inhibits hepatic FGF21 expression via LPA-induced ERK activation and subsequent PPARα suppression.

FGF21 Is an Obligatory Mediator for the Therapeutic Benefits of Anti–ATX Antibody Against Steatosis, NASH, and Fibrosis

FGF21 analogs and agonists have been shown to be highly effective in ameliorating NAFLD in both animal
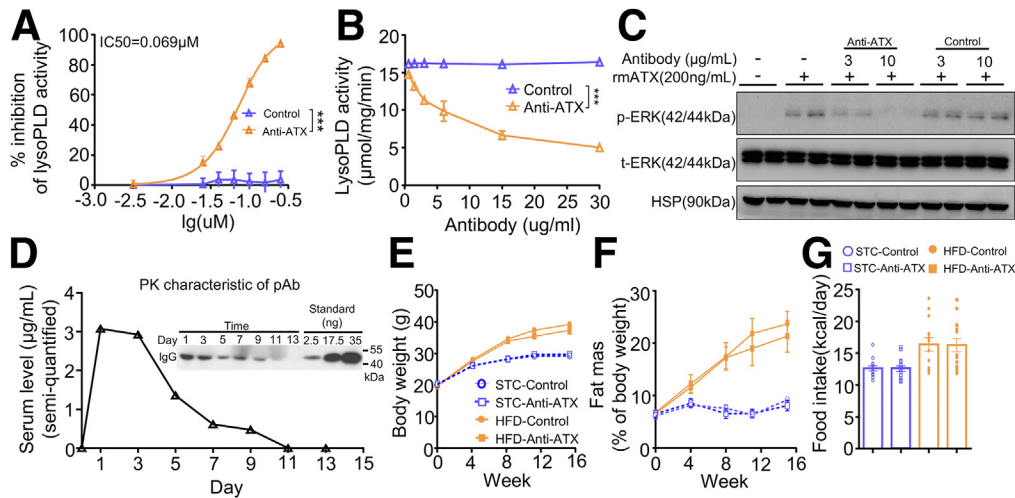
Figure 5. Characterization of the neutralizing activity of anti-autotaxin IgG and evaluation of its effects on body weight, fat mass, and food intake in mice. (*A*) Concentration-dependent response curves for the inhibitory effect of anti-mouse autotaxin IgG (anti-ATX) on serum lysoPLD activity (shown as the percentage of inhibition). Rabbit nonimmune IgG (Control) was used as a control. The sera used were from 6-week-old C57BL/6N male mice (n = 3 from each time point). (*B*) Concentration-dependent effects of anti-ATX IgG on lysoPLD activity of rmATX (n = 3 from each time point). (*C*) Dose-dependent effect of anti-ATX IgG on autotaxin-induced phosphorylation of the MAP kinase ERK1/2 in HepG2 cells. Cells grown in serum-free medium with the addition of 50 μmol/L 14:0 lysophosphatidylcholine were treated without or with 200 ng/mL rmATX in the absence or presence of different concentrations of anti-ATX or nonimmune IgG for 10 minutes and then were harvested for Western blot analysis (n = 3 in each group). HSP90 was used as a loading control. (*D*) Dynamic changes in circulating anti-ATX IgG after a single intravenous injection (1 mg/kg body weight) into 14-week-old C57BL6/N mice (n = 4) measured with Western blot (*insert*). For the determination of serum levels of anti-ATX neutralizing IgG, a standard curve was generated by densitometry using a series of rabbit nonimmune IgG standards with known quantity, and the concentration of anti-ATX neutralizing IgG was calculated based on the equation generated from the standard curve. ***$P < .001$. Data are presented as the means ± SEM. (*E–G*) Six-week-old C57BL/6N male mice (n = 6–8) were fed with either STC or HFD for 8 weeks, and subsequently injected with 1 mg/kg body weight anti-ATX or nonimmune IgG (control) every 10 days for another 7 weeks (5 injections in total). (*E*) Body weight and (*F*) fat mass were measured at the indicated time points; (*G*) average daily food intake is shown as kilocalories per day. Data are presented as the means ± SEM. (*E–G*) Statistical calculations were performed by 1-way analysis of variance followed by Tukey multiple comparisons using Prism 6. (*A* and *B*) Statistical calculations were performed by the Student *t* test using Prism 6. IC50, half maximal inhibitory concentration; pAb, polyclonal antibody; p-ERK, phosphorylated extracellular signal-related kinase; PK, pharmacokinetics; t-ERK, total extracellular signal-related kinase; MAP, mitogen-activated protein.

models and patients.[8,43] We next investigated whether the therapeutic effect of autotaxin neutralization on fatty liver requires hepatic up-regulation of FGF21 using FGF21 knockout mice.[44,45] Treatment with anti-ATX IgG led to a comparable degree of suppression on lysoPLD activity in HFD-fed FGF21 knockout mice and WT littermates (Figure 8*A*). However, the effects of anti-ATX IgG on improvement of serum lipid profiles, reduction of liver weight, and alleviation of hepatic steatosis and liver injury were observed only in WT mice, but not in FGF21 knockout mice (Figure 8*B–F*). Similarly, anti-ATX IgG induced up-regulation of FAO-related genes, increases in hepatic FAO activity, and in serum adiponectin levels were blunted markedly in FGF21 knockout mice (Figure 8*G–I*), supporting the role of FGF21 as an indispensable downstream effector conferring hepatoprotective effects of anti-ATX IgG in obese mice.

In light of the fact that recent clinical trials have shown promising therapeutic potential of FGF21 analogs for patients with NASH and fibrosis,[8,43,46] we next explored whether neutralization of autotaxin with anti-ATX IgG ameliorates advanced stages of NAFLD in choline-deficient,

L-amino acid–defined, 60% HFD (CDAHF60)-fed mice, which develop all of the histologic features of NAFLD, including severe steatosis, inflammation, and fibrosis.[47,48] Although CDAHF60 feeding did not increase body weight and fat mass, it caused a time-dependent increase in the serum level of autotaxin and its lysoPLD activity, as well as the autotaxin mRNA expression in the liver but not in adipose tissue, as compared with age-matched STC-fed mice (Figure 9*A–C* and *E–G*). The typical histopathology of NAFLD and liver injury were readily detected at 4 weeks after feeding CDAHF60 (Figure 9*D*). Treatment with anti-ATX IgG led to a comparable reduction in circulating lysoPLD activity between FGF21 knockout mice and WT littermates (Figure 10*A*), and markedly increased serum FGF21 levels in WT mice, but not in FGF21 knockout mice (Figure 10*B*). Notably, the significant effects of anti-ATX antibody on amelioration of serum triglycerides, cholesterol, and FFAs, and increase of serum adiponectin were observed only in WT mice, but not in FGF21 knockout mice (Figure 10*C* and *D*). Furthermore, anti-ATX IgG significantly decreased liver weights, attenuated steatosis inflammation, fibrosis, and NASH scores (NAFLD Activity Score, NAS) as determined by
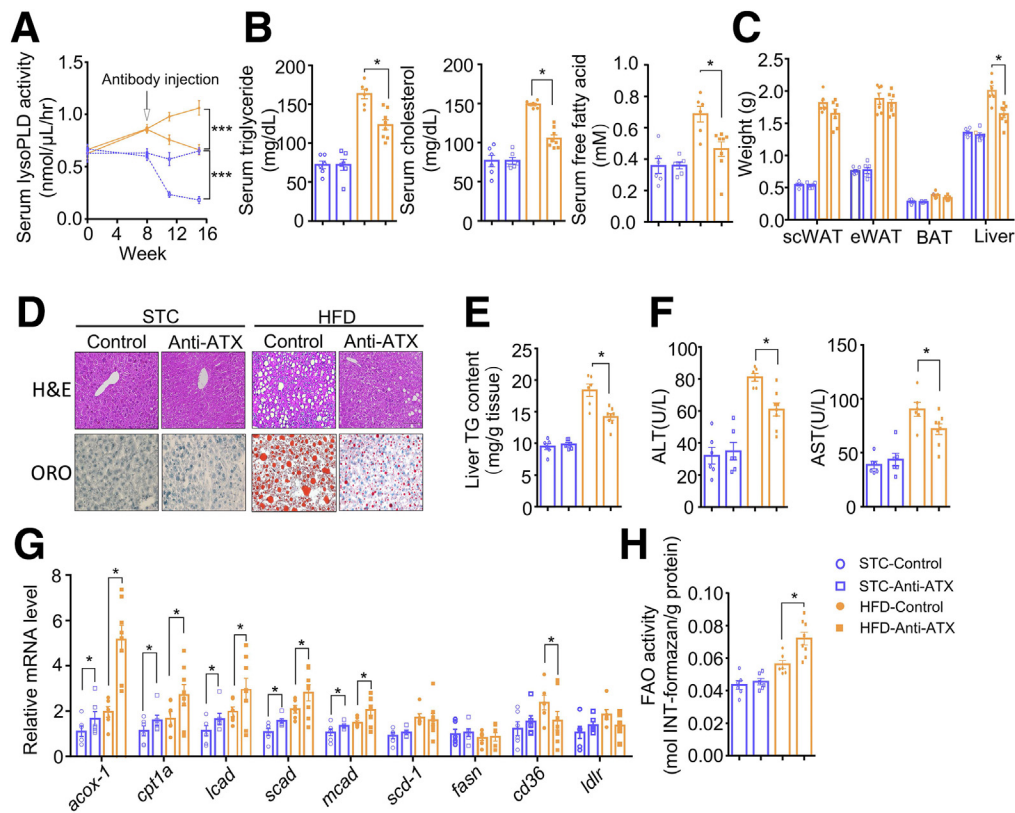
Figure 6. Treatment of anti-autotaxin neutralizing antibody ameliorates obesity-induced dyslipidemia and NAFLD. Six-week-old C57BL/6N male mice (n = 6–8) were fed with either STC or HFD for 8 weeks, and subsequently injected with 1 mg/kg body weight antibody (anti-ATX or nonimmune IgG [control]) every 10 days for another 7 weeks (5 intravenous injections in total). Mice were killed at the 15th week. (*A*) Serum lysoPLD activity at different time points. (*B*) Serum levels of triglyceride (TG), cholesterol, and free fatty acid levels. (*C*) Wet weight of different organs. (*D*) Representative photos of H&E staining and Oil Red O (ORO) staining of liver sections (200×; *scale bar*: 200 um), (*E*) hepatic triglyceride content, and (*F*) serum levels of ALT and AST. (*G*) Real-time PCR analysis for genes involved in hepatic lipid metabolism. Genes were normalized with β-*actin* and shown as the fold change against the STC–Control group. (*H*) The FAO rate in livers. Oxidation of fatty acid was coupled to reduced nicotinamide adenine dinucleotide–dependent reduction of INT to INT-formazan. FAO activity was shown as the production of INT-formazan (mol) per gram protein. n = 6–8. (*A–C* and *E–H*) Statistical calculations were performed by 1-way analysis of variance followed by Tukey multiple comparisons using Prism 6. *$P < .05$ and ***$P < .001$. Data are presented as the means ± SEM. BAT, brown adipose tissue; eWAT, epididymal adipose tissue; scWAT: subcutaneous adipose tissue.

histologic examination (Figure 10*E–G*), obviously reduced triglyceride accumulation in the liver and serum levels of ALT and AST (Figure 10*H* and *I*), improved FAO rate (Figure 10*J*), and inhibited the expression of several fibrosis-related genes including *Acta2*, *Col1a1*, *Timp-1*, and *Fn1* (Figure 10*K*). However, all of these therapeutic benefits of anti-ATX IgG on NASH and fibrosis was largely abolished in FGF21 knockout mice, indicating that anti-ATX IgG–mediated neutralization of autotaxin is effective in treating CDAHF60-induced NASH and fibrosis by induction of FGF21.

Discussion

In the present study, we provide both clinical and experimental evidence that increased autotaxin is an important contributor to the pathogenesis of NAFLD through LPA-induced inhibition of PPARα. Furthermore, small interfering RNA–mediated blockage of hepatic autotaxin production or treatment with an antibody that neutralizes the lysoPLD activity of autotaxin potently ameliorates fatty liver, NASH, and hepatic fibrosis in 2 different mouse models with NAFLD by promoting FGF21 production (Figure 11). These findings identify the ATX–LPA axis as an endogenous inhibitor of hepatic FGF21 expression, and a promising therapeutic target for the treatment of NAFLD.

The ATX–LPA axis regulates a plethora of cellular functions including proliferation and growth, development, chemotaxis, vasoregulation, calcium dynamics, and energy homeostasis by binding LPA to its G-protein–coupled receptors (LPA1-6).[36] Augmented autotaxin expression has been implicated in multiple types of cancers, chronic inflammatory diseases, and cardiomyopathy.[49–51] Although autotaxin previously was thought to be an adipokine expressed abundantly in adipose tissue in rodents, our present study shows that liver, but not adipose tissue, is a major contributor to increased circulating autotaxin in both

human beings and several types of mouse models with NAFLD. In obese subjects, autotaxin expression in liver is much higher than in visceral and subcutaneous adipose tissues. Furthermore, autotaxin expression in liver, but not in adipose tissues, correlates strongly with serum autotaxin, which is closely associated with several histopathologic features as well as staging of biopsy-proven NAFLD. In a *lipodystrophic mouse* model without adipose tissues, circulating autotaxin remains increased owing to its markedly increased hepatic expression. Furthermore, in NAFLD

mouse models induced by both dietary obesity and CDAHF60 diet, autotaxin expression is increased markedly in liver but remains little changed in other tissues, while selective knockdown of hepatic autotaxin expression alone is sufficient to counteract dietary obesity and a CDAHF60-induced increase of circulating autotaxin, accompanied with obvious amelioration of NAFLD and liver injury. Taken together, these findings support the causal role of liver-secreted autotaxin in the development of NAFLD in both animals and human beings. In line with our finding, a
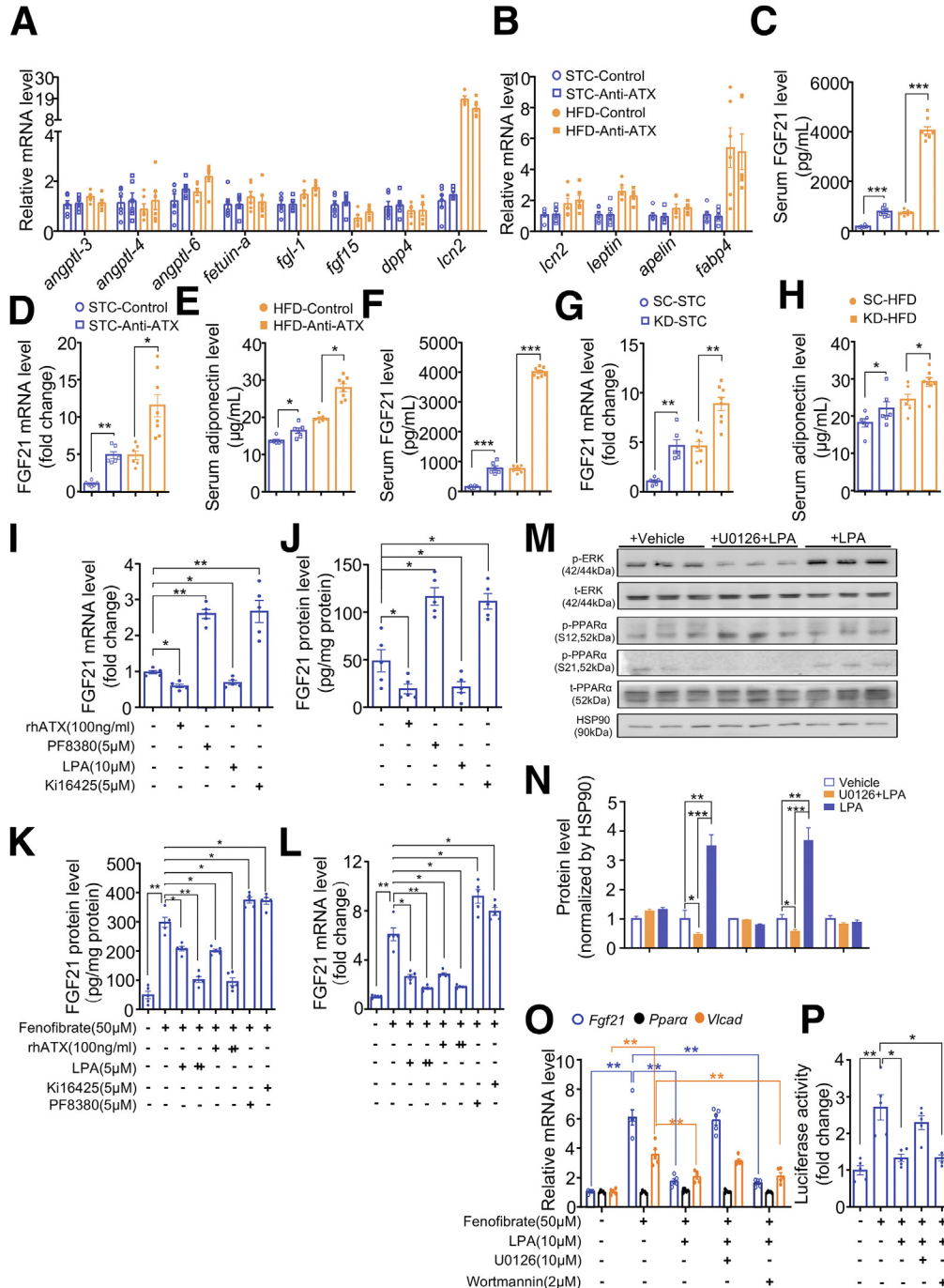
previous study found that hepatocyte-secreted autotaxin contributes to lipid accumulation and carcinogenesis in the liver in a N-nitrosodiethylamine/carbon tetrachloride (DEN/CCL4) induced hepatocellular carcinoma mouse model.[16]

FGF21, a hormone secreted predominantly from hepatocytes, possesses pleiotropic protective activities against obesity and its related metabolic complications including NAFLD.[8,46,52,53] In mice, FGF21 knockout exacerbates methionine and choline-deficient diet–induced hepatic steatosis, inflammation, and fibrosis,[44,54] while treatment with recombinant FGF21 or its analogs markedly ameliorates these pathologic changes in the liver of both mice and rodents.[44,54] FGF21 has been shown to exert its hepatoprotective effects through its direct actions in the liver by promoting fatty acid oxidation, enhancing hepatic insulin sensitivity, attenuating endoplasmic reticulum and oxidative stresses,[8,52,53] limiting endotoxin-induced liver inflammation and injury, blocking nuclear factor-κB,[55] and mitigating fibrogenic gene expression in hepatic stellate cells.[56] Furthermore, administration of FGF21 or its analogs in both mice and human beings induces the production of adiponectin, an adipokine with insulin-sensitizing, anti-inflammatory, and hepatoprotective properties.[33] Notably, several recent clinical trials have shown highly promising therapeutic benefits of FGF21 analogs (such as pegylated long-acting forms of FGF21) and FGF21-receptor agonists in the treatment of biopsy-confirmed NASH patients.[8,43,46,57,58] In another clinical study with biopsy-confirmed F1–F3 NASH patients, treatment with efruxifermin (a long-acting FGF21 fusion protein with fragment crystallizable (Fc) fragment) lead to a more than 70% reduction in liver fat contents, accompanied by resolution of histologic features of NASH and fibrosis, reduction of liver injury, and increase of adiponectin (NCT05039450).[59] A remarkable reduction in liver fat content and markers of liver fibrosis and injury also have been observed in obese adults treated with another genetically engineered FGF21 analogue: LLF580.[60] In the present study, we observed a marked increase in both circulating levels of FGF21 and its hepatic expression in both dietary obese mice and CDAHF60-fed mice with autotaxin knockdown or antibody neutralization, while the effects of knocking down or neutralizing autotaxin in ameliorating steatosis, NASH, and fibrosis, and in promoting hepatic fatty acid oxidation, largely were abrogated in FGF21 knockout mice, suggesting that increase of endogenous FGF21 production by pharmacologic or genetic inhibition of hepatic autotaxin may represent another therapeutic approach for treatment of NAFLD by targeting FGF21.

Another notable finding of our study was that the ATX–LPA axis acts in an autocrine manner to suppress PPARα activity, which is a master regulator of hepatic lipid metabolism and an obligatory transcription factor for hepatic FGF21 production.[37,38,61] In Huh7 hepatocytes, both autotaxin and LPA dose-dependently inhibit fenofibrate-induced PPARα activation and FGF21 production, possibly through ERK1/2-induced Ser21 phosphorylation of PPARα located within the A/B domain of PPARα, and such effects are reversed by pharmacologic inhibition of autotaxin or ERK. In line with our findings, ERK-induced phosphorylation and deactivation of PPARα has been implicated in cardiac hypertrophic growth and myocadiac lipid accumulation.[42] However, another study reported that PPARα can be activated by ERK1/2 in response to insulin or Pseudomonas aeruginosa stimulation in lung epithelial cells,[40,41] suggesting that ERK regulates PPARα activity in a cellular context-dependent manner. PPARα decreases triglycerides by

---

Figure 7. The ATX–LPA axis suppresses hepatic production of FGF21 via ERK-mediated inhibition of PPARα. Six-week-old C57BL/6N male mice (n = 6–8) were fed with either STC or HFD for 8 weeks, and subsequently injected with 1 mg/kg body weight antibody (anti-ATX or nonimmune IgG [control]) every 10 days for another 7 weeks as in Figure 6. Mice were killed at the 15th week. (A) Real-time PCR analysis of mRNA expression levels of several hepatokines in liver (shown as fold change against the STC–Control group). (B) Real-time PCR analysis for mRNA expression levels of several adipokines in epididymal adipose tissue (shown as fold change against the STC–Control group). n = 6–8. Data are presented as the means ± SEM. (C) Serum levels of FGF21. (D) Hepatic mRNA expression levels of Fgf21 determined by real-time PCR analysis. (E) Serum levels of adiponectin. (F–H) Six-week-old C57BL/6N male mice were fed with STC or HFD for 15 weeks after intravenous injection with 1×10^{11} vector genome of AAV encoding shRNA specific to autotaxin (KD) or scramble control (SC) as in Figure 4. (F) Serum levels of FGF21. (G) Hepatic mRNA expression levels of FGF21 determined by real-time PCR analysis. (H) Serum levels of adiponectin. (I–J) Huh7 cells grown in serum-free DMEM were treated with or without the indicated dosage of rhATX, PF8380 (inhibitor of autotaxin), LPA, or Ki16425 (LPA-receptor antagonist) for 24 hours. (I) The mRNA expression levels of FGF21 (expressed as fold changes relative to vehicle [dimethyl sulfoxide]-treated controls) and its (J) protein concentrations in the conditioned medium were determined by real-time PCR and enzyme-linked immunosorbent assay (ELISA), respectively. n = 5. Data are presented as the means ± SEM. (K–L) Huh7 hepatocytes were pretreated with rhATX, LPA, PF8380 (inhibitor of autotaxin), Ki16425 (LPA-receptor antagonist) for 30 minutes, followed by treatment with or without fenofibrate for 24 hours. (K) FGF21 protein was secreted into conditioned medium and (L) hepatic FGF21 mRNA were determined by ELISA and real-time PCR, respectively. Huh7 hepatocytes were pretreated with U0126 (ERK inhibitor), wortmannin (PI3K), or LPA for 30 minutes, (M and N) followed by treatment with or without fenofibrate for 30 minutes to collect cell lysates for Western blot analysis, or (O) 24 hours to measure the relative mRNA abundance of FGF21, PPARA, and VLCAD (very-long-chain acylcoenzyme-A dehydrogenase, a downstream target of PPARα). (P) Relative luciferase activity in Huh7 hepatocytes transfected with a luciferase reporter vector carrying PPAR response element and treated with LPA, U0126, and wortmannin in the presence or absence of fenofibrate for 48 hours. Data are normalized against human β-ACTIN and expressed as the fold change relative to dimethyl sulfoxide–treated controls. (A–L and N–P) Statistical calculations were performed by 1-way analysis of variance followed by Tukey multiple comparisons using Prism 6. *$P < .05$, **$P < .01$, and ***$P < .001$. n = 5. Data are presented as the means ± SEM. HSP90, heat shock protein 90; p-ERK, phosphorylated_extracellular signal-related kinase; p-PPARα, phosphorylated peroxisome proliferator–activated receptor α; t-ERK, total extracellular signal-related kinase; t-PPARα, total peroxisome proliferator–activated receptor α.
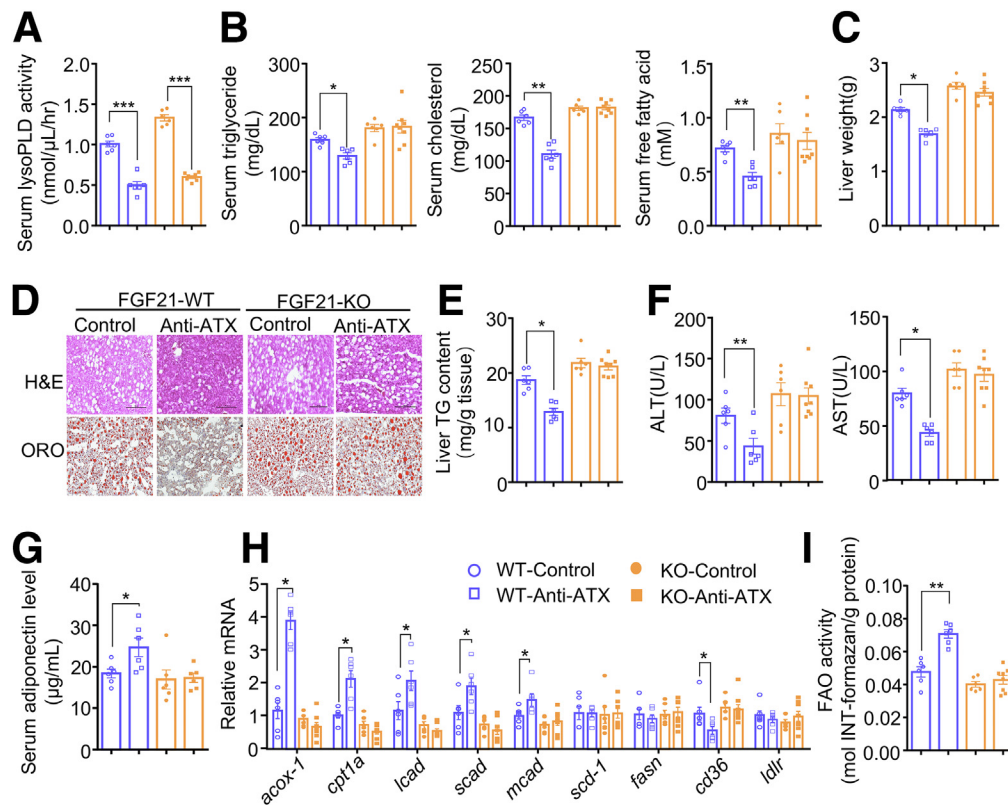
Figure 8. FGF21-deficient mice are refractory to the therapeutic benefits of anti-autotaxin antibody against obesity-induced dyslipidemia and fatty liver. Six-week-old male FGF21 KO mice in a C57BL/6N background and their WT littermates (n = 6–8) were fed with HFD for 8 weeks, and subsequently treated with 1 mg/kg body weight anti-ATX (IgG or nonimmune IgG [control]) every 10 days for another 7 weeks by 5 intravenous injections as in Figure 3. (A) Serum lysoPLD activity. (B) Serum levels of triglyceride, cholesterol, and free fatty acid. (C) Wet weight of liver tissues. (D) Representative images of H&E staining and Oil Red O (ORO) staining of liver sections (200×; *scale bar*: 200 um). (E) Hepatic triglyceride content. (F) Serum levels of ALT and AST. (G) Serum adiponectin levels. (H) Real-time PCR analysis for genes involved in hepatic lipid metabolism. Genes are normalized with β-actin and shown as the fold change against the WT–Control group. (I) The FAO rate in livers. Oxidation of fatty acid was coupled to reduced nicotinamide adenine dinucleotide–dependent reduction of INT to INT-formazan. FAO activity was shown as production of INT-formazan (mol) per gram protein. n = 6–8. (A–C and E–I) Statistical calculations were performed by 1-way analysis of variance followed by Tukey multiple comparisons using Prism 6. *$P < .05$, **$P < .01$, and ***$P < .001$. Data are presented as the means ± SEM.

transactivation of a cluster of genes involved in fatty acid metabolism and ketogenesis, in which FGF21 acts as an obligatory downstream effector.[37,61–64] Mice with global and hepatocyte-specific PPARα are more susceptible to HFD-induced hepatic steatosis and methionine/choline-deficient diet–induced NASH,[65] while treatment with PPARα agonists ameliorates hepatic steatosis and inflammation in several different types of NAFLD mouse models.[66,67] However, clinical trials failed to show any therapeutic benefits of either PPARα agonists or a PPARα/δ agonist on liver histology in NASH patients despite significant improvements in circulating lipid profiles (NCT02704403),[68] suggesting that PPARα activation alone is insufficient for the treatment of NAFLD. In this connection, an augmented ATX–LPA axis has been linked to several pathophysiological pathways involved in NAFLD development, including exacerbation of proinflammatory responses,[69] induction of insulin resistance,[18,49] apoptosis,[70] and fibrosis[15,16,71] in different disease models. Therefore, pharmacologic interventions

targeting autotaxin are expected to produce additional therapeutic benefits beyond PPARα activation and FGF21 production and may represent a more efficacious strategy for treatment of NAFLD.

A large number of chemical inhibitors of autotaxin and LPA-receptor antagonists have been developed recently for the treatment of different chronic diseases, such as idiopathic pulmonary fibrosis, systemic sclerosis, and neurodegenerative diseases.[36] However, several clinical trials on the inhibitors of autotaxin (such as GLPG1690) and lysophosphatidic acid receptor antagonist (such as BMS-986020) were terminated because of severe adverse effects of these chemical compounds (https://clinicaltrials.gov).[72] Therapeutic antibodies have several advantages over small-molecule drugs with respect to target specificity, safety, and stability. In this connection, our study provides proof-of-concept evidence that antibody-mediated neutralization of autotaxin activity is highly efficacious in ameliorating fatty liver and NASH in 2 different mouse models,
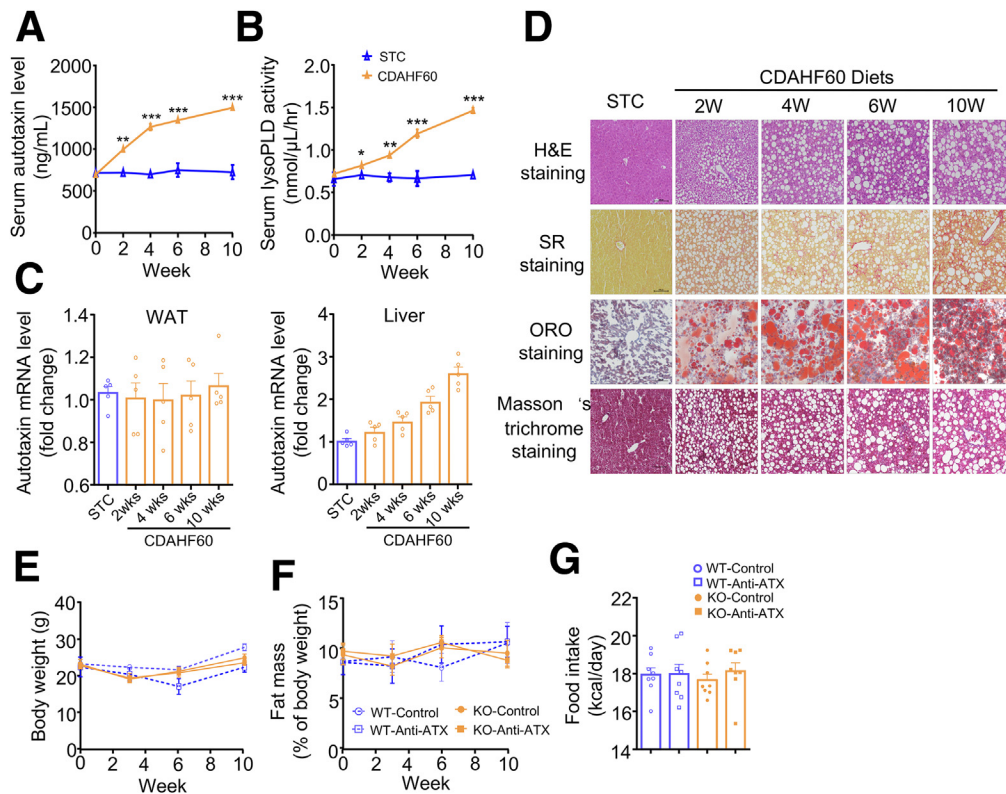
Figure 9. Dynamic changes of autotaxin expression in mice with CDAHF60 diet-induced NASH. Ten-week-old C57BL/6N male mice were fed with STC or CDAHF60 diet for 10 weeks (n = 5/time point). (*A*) Serum autotaxin levels and (*B*) serum lysoPLD activity measured at different time points after initiation of CDAHF60 diet. (*C*) Real-time PCR analysis for mRNA expression levels of autotaxin in liver and epididymal white adipose tissue were expressed as fold changes relative to STC group. (*D*) Representative images of liver sections showing the histopathologic development of CDAHF60-induced NASH, as evaluated by H&E, Oil Red O (ORO), Sirius red, and Masson's trichrome staining. *Scale bar*: 100 μm. (*E–G*) Ten-week-old male FGF21 KO mice and their WT littermates fed on CDAHF60 diet for 3 weeks were treated with anti-ATX or nonimmune IgG (1 mg/kg body weight, 5 injections) every 10 days for 7 weeks upon CDAHF60 diet feeding (n = 6–8). (*E*) Body weight and (*F*) fat mass were measured at the indicated time points; (*G*) average daily food intake is shown as kilocalories per day. (*A* and *B*) Statistical calculations were performed by the Student *t* test using Prism 6. (*C* and *E–G*) Statistical calculations were performed by 1-way analysis of variance followed by Tukey multiple comparisons using Prism 6. *$P < .05$, **$P < .01$, and ***$P < .001$. Data are presented as the means ± SEM. SR, Sirius Red.

suggesting that the neutralizing antibodies against autotaxin may represent a promising strategy for drug development.

Methods

Study Approval

The human study was approved by the Institutional Review Board of Jinan University (2016-017) and the University of Hong Kong/Hospital Authority Hong Kong West Cluster (UW 20-700), and conducted according to Declaration of Helsinki principles. Written informed consent was received from participants before their inclusion in the study. Animal studies were approved by the Committee on the Use of Live Animals in Teaching and Research at the University of Hong Kong.

Clinical Studies

A total of 151 obese patients were recruited consecutively from the Bariatric Surgery Clinic at the First Affiliated Hospital of Jinan University. Overweight and obesity class were classified by BMI, according to the World Health Organization Asian Standard. Overweight, class I obesity, and class II

obesity were defined as a BMI of 23.0–24.9 kg/m^2, BMI of 25–29.9 kg/m^2, and BMI $\geq$30 kg/m^2, respectively. Twenty-six individuals were excluded because of the following reasons: (1) age younger than age 18 years; (2) had syphilis or human immunodeficiency virus infection; (3) heavy alcohol drinking history ($\geq$40 g/d for up to 2 weeks); and (4) lack of sufficient information. Demographic, clinical, and laboratory data (after an overnight fast of at least 10 hours) for each patient were collected within 1 week before their surgery and liver biopsy specimens were obtained during the bariatric surgery. Liver biopsy specimens were taken from the middle of the right lobe during bariatric surgery. Thin sections of liver biopsy specimens were stained with H&E or Masson trichrome, and were evaluated by 3 independent experienced liver pathologists (Dr Subrata Chakrabarti, Western University, London, Ontario, Canada; Dr Hema Mahajan, Western Sydney University, Greater Western Sydney, New South Wales, Australia; and Dr Sen Yan, Dr Everett Chalmers Hospital, New Brunswick, Canada). The scores of steatosis (0–3), hepatocellular ballooning (0–2), lobular inflammation (0–3), and fibrosis (0–4) were
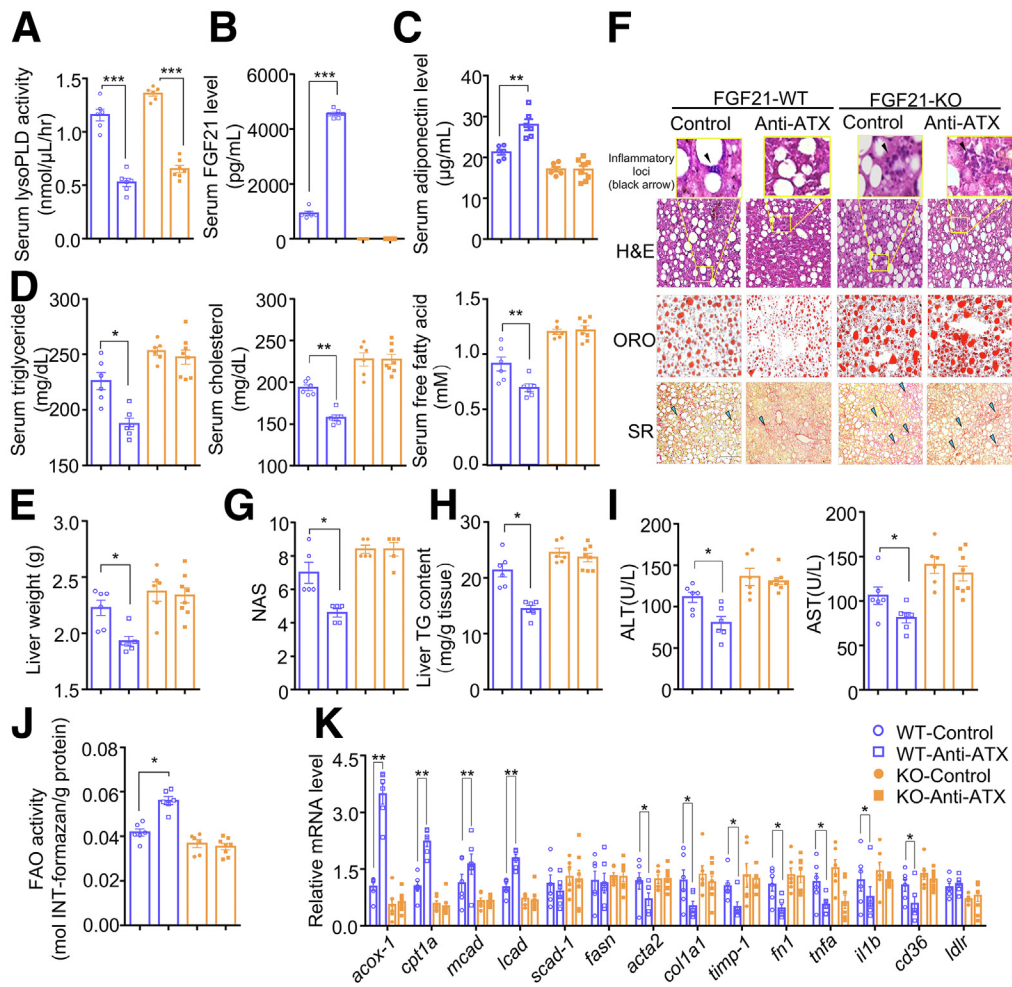
Figure 10. Anti-autotaxin neutralizing antibody alleviates CDAHF60 diet-induced NASH by inducing FGF21 production. Ten-week-old male FGF21 KO mice and their WT littermates were fed with choline-deficient, L-amino acid–defined, 60% high-fat (CDAHF60) for 3 weeks, followed by 5 intravenous injections of 1 mg/kg body weight anti-ATX (or nonimmune IgG [Control]) every 10 days for 7 weeks upon CDAHF60 feeding. (*A*) Serum lysoPLD activity in mice. Serum levels of (*B*) FGF21 and (*C*) adiponectin. (*D*) Serum concentrations of triglycerides, cholesterol, and free fatty acids. (*E*) Liver weights. (*F*) Representative photographs of inflammatory loci (shown as 4× magnified photos of H&E, indicated by *black arrowheads*), H&E, Oil Red O (ORO), and Sirius red staining of liver sections (200×; *scale bar*: 200 um). *Blue arrowheads*: collagen formation. (*G*) NASH scores (NAFLD activity score, NAS) as determined by histologic examination. (*H*) Hepatic triglyceride content. (*I*) Serum levels of ALT and AST. (*J*) FAO rate in livers. Oxidation of fatty acid was coupled to reduced nicotinamide adenine dinucleotide–dependent reduction of INT to INT-formazan. FAO activity was shown as production of INT-formazan (mol) per gram protein. (*K*) Real-time PCR analysis of genes involved in hepatic lipid metabolism (*Cpt1a, Acox1, L/M/Scad, Scd-1, Fasn, Cd36, Ldlr*); fibrosis and inflammatory responses (*Acta2, Col1a1, Timp-1, Fn1, Tnfa, Il1b*). Genes were normalized with β-actin and shown as the fold change relative to WT–control group. n = 6–8. (*A–E* and *G–K*) Statistical calculations were performed by 1-way analysis of variance followed by Tukey multiple comparisons using Prism 6. *$P < .05$, **$P < .01$, and ***$P < .001$. Data are presented as the means ± SEM.

evaluated according to the NASH Clinical Research Network scoring system.[73] For measurement of autotaxin mRNA and protein levels, biopsy specimens of intra-abdominal (visceral) and subcutaneous adipose tissues and liver obtained during bariatric surgery were immediately frozen in liquid nitrogen and stored at $-80°$C. Serum was isolated by centrifugation, and immediately stored at $-80°$C for further analysis.

Animal Experiments

C57BL/6N mice were obtained from the Animal Unit of the University of Hong Kong. Mice were housed at a controlled

temperature ($23°$C $\pm$ $1°$C) with a 12-hour light/12-hour dark cycle and free access to drinking water and different types of diet: standard chow (catalog #5053, LabDiet, St. Louis, MO), rodent high-fat diet with 45 kcal% fat (D12451, Research Diets), or L-amino acid rodent diets with 60 kcal% fat with low methionine and no added choline diet (CDAHF60, Dyets). Fgf21 KO mice and their WT littermates in C57BL/6N were generated as previously described.[33,74] Genotyping was conducted as previously described.[45] Adipocyte-specific MDM2 KO mice were generated by crossing MDM2^floxed/floxed^ mice with Adipoq-Cre mice (expressing Cre recombinase under the control of the adiponectin promoter; The Jackson Laboratory, Bar

Figure 11. Schematic summary of the role of hepatocyte-secreted autotaxin in exacerbating NAFLD through its autocrine actions. Obesity or other risk factors promote increased production and secretion of autotaxin, thereby catalyzing the conversion of lysophosphatidylcholine (LPC) to LPA, which in turn binds to its receptors (LPARs) to trigger ERK activation and subsequent PPARα inhibition, leading to decreased production of FGF21 and adiponectin. Anti-autotaxin neutralizing antibodies reverse these pathologic pathways and increase FGF21 production, thereby exerting its therapeutic benefits on alleviation of hepatic steatosis, steatohepatitis, and fibrosis. p-Erk, phosphorylated_extracellular signal-related kinase; PPRE, peroxisome proliferator response element.
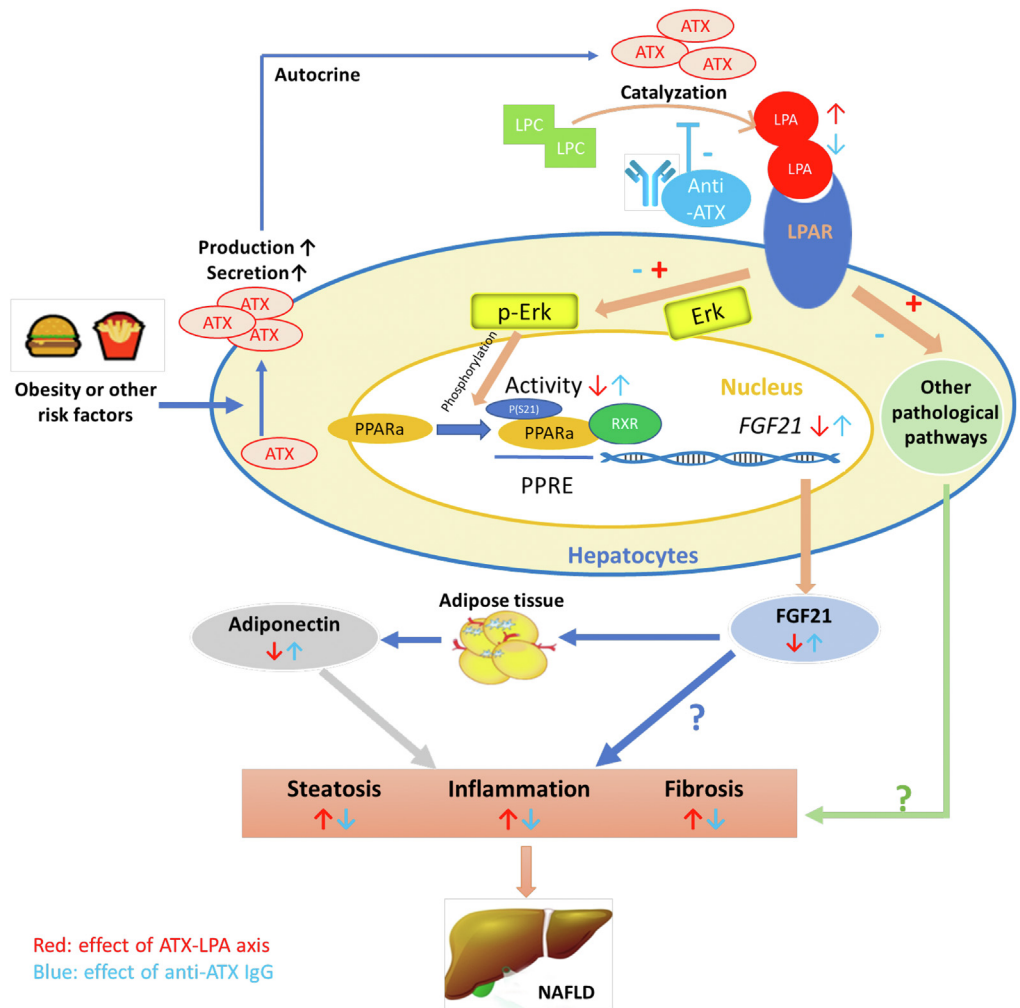
Harbor, ME) as previously described.[31] Mice were subjected to AAV infection or antibody treatment as indicated in each figure legend. Body composition was determined by the Bruker Minispec LF90 II Body Composition Analyzer (Bruker Biospin, Billerica, MA). Food intake was measured every week and shown as the calculated average daily calorie intake per mouse.

Histologic Analysis and Oil Red O Staining

A liver specimen (approximately 5 mm × 5 mm) taken from the right lobe near the portal vein was fixed in 4% (w/v) paraformaldehyde, dehydrated, and embedded in paraffin as previously described.[75] The paraffin-embedded liver sections (5 μm) were deparaffinized, rehydrated, and stained with H&E, Sirius Red (Picro Sirius Red Staining Kit, ab150681; Abcam, Cambridge, UK), or Trichrome Stain (Masson's) (SDHT15; Sigma-Aldrich, Burlington, MA) according to the manufacturer's instructions. For Oil Red O staining, liver embedded in optimal cutting temperature compound (OCT compound) was immediately frozen on dry ice. Frozen sections (7 μm) were obtained using a Leica CM 1900 Cryostat (Leica Biosystems, Nussloch, Germany). Rehydrated sections were rinsed with 60% isopropanol and stained for 20 minutes with 0.3% Oil Red O solution,

followed by rinsing 3 times in 60% isopropanol and twice in double-distilled water. Slides were further counterstained with hematoxylin and mounted.

Immunoblot Analysis and Real-Time PCR

Proteins were isolated from cells or various mouse tissue using radioimmunoprecipitation assay buffer (150 mmol/L sodium chloride, 1.0% NP-40, 0.5% sodium deoxycholate, 0.1% sodium dodecyl sulfate, 50 mmol/L Tris, pH 8.0) containing protease inhibitor cocktail (0469315900; Roche, Basel, Switzerland), separated by sodium dodecyl sulfate–polyacrylamide gel electrophoresis, transferred to polyvinylidene difluoride membranes, and incubated with various primary antibodies at 4°C overnight, using horse-radish-peroxidase–linked anti-rabbit IgG (7074; Cell Signaling Technology, Beverly, MA) as a secondary antibody. The following primary antibodies were used for immuno-blot analysis: heat shock protein 90 (HSP90, #4874S), Erk1/2 (#9102s), phospho-Erk1/2 (#9101S) from Cell Signaling Technology Danvers, MA); PPARα (phospho S12) (#ab3484) from Abcam (Abcam, Cambridge, UK); phospho-PPARα (#AF8054) from Affinity Biosciences (OH); and PPARα (sc-398394) from Santa Cruz (CA). The protein bands were

visualized by enhanced chemiluminescence reagents (GE Healthcare) and quantified using ImageJ software (National Institutes of Health, Bethesda, MD) based on the intensities of bands. For the determination of serum levels of anti-ATX neutralizing IgG, a standard curve was generated by densitometry using a series of rabbit nonimmune IgG standards with known quantity, and concentration of anti-ATX neutralizing IgG was calculated based on the equation generated from the standard curve.

Total RNA was extracted from cells or various mouse tissues using TRIzol (Invitrogen, Waltham, MA) following the manufacturer's instructions and subsequently reverse-transcribed into complementary DNA using a reverse-transcription kit (PrimeScript RT reagent kit, RR037A; Takara, Kusatsu, Shiga, Japan). Real-time PCR was performed using SYBR Green master mix (RR420D; Takara) on the Applied Biosystems Prism 7000 sequence detection system (Thermo Fisher Scientific, Waltham, MA), using the primers listed in Table 3. All mouse genes were normalized against the mouse β-actin gene and human genes were normalized against the human β-actin gene.

Liver Fractionation

Liver fractionation was performed as previously described.[76] In brief, liver was perfused with ethylene glycol-bis(β-aminoethyl ether)-N,N,N′,N′-tetraacetic acid solution (calcium-free Hank's balanced salt solution with 25 mmol/L HEPES and 0.2 g/L ethylene glycol-bis(β-aminoethyl ether)-N,N,N′,N′-tetraacetic acid) and sequentially perfused with digestion solution (Iscove's modified Dulbecco's medium with GlutaMAX (35050061; Thermo Fisher Scientific), 500 mg/L collagenase type 4) under a warming infrared light. The liver then carefully was removed from the abdominal cavity and placed in a Petri dish filled with 5 mL postdigestion solution (Dulbecco's modified Eagle medium [DMEM] with GlutaMAX, 25 mmol/L HEPES, and 10% fetal bovine serum [FBS]) and was mechanically disrupted by a scalpel blade. Minced liver was collected and diluted with 45 mL postdigestion solution into a 50-mL conical tube on ice. The suspension was passed through a 70-μm cell strainer and centrifuged at $68 \times g$ for 5 minutes. The pellet then was washed with phosphate-buffered saline 2 times at $68 \times g$ for 10 minutes to obtain parenchymal cells. The top 40 mL was transferred into a new tube and centrifuged at $460 \times g$ for 10 minutes. The pellet was resuspended in 37.5% Percoll (P1644; Sigma) containing 5 mmol/L EDTA, followed by centrifugation at $850 \times g$ for 30 minutes. The pellet was resuspended in red cell lysis buffer (00-4333-57; Invitrogen), followed by centrifugation at $460 \times g$ for 10 minutes to collect nonparenchymal cells in the pellets.

Biochemical and Immunologic Analyses

Mouse autotaxin, FGF21, and adiponectin were measured with enzyme-linked immunosorbent assay kits (32770, 32180, and 32010, respectively; Immunodiagnostics, Ltd, Hong Kong, China). Serum levels of human FGF21 and human autotaxin were quantified with enzyme-linked immunosorbent assay kits (31180 and 31770, respectively; Immunodiagnostics, Ltd). Serum FFAs were determined by a FFA Half Micro Test kit (Roche). Serum triglyceride, cholesterol, ALT, and AST levels were measured using commercial kits from STANBIO Laboratory (Kolkata, West Bengal, India). To measure liver triglyceride content, liver tissues ($\sim$50 mg) were homogenized in chloroform/methanol (2:1 v/v) using a tissue homogenizer. Lipid extracts were prepared by the Folch method, as previously described,[77] and then were dried under nitrogen flow and further dissolved in ethanol. The FAO rate was measured using a commercial kit (E-141; Biomedical Research Service, University at Buffalo, Buffalo, NY) following the manufacturer's instructions.[78,79] The FAO activity assay is based on the oxidation of octanoyl-CoA (an intermediate during β-oxidation). Generation of reduced nicotinamide adenine dinucleotide in this reaction is coupled to the reduction of the tetrazolium salt INT to formazan. The intensity of the red-colored formazan is proportional to FAO activity. Briefly, 10 mg liver tissue was lysed in 200 uL lysis buffer (provided in the kit) and incubated on ice for 5 minutes, followed by centrifugation at $11,000 \times g$ for 5 minutes at $4°C$. The supernatant was transferred to a new tube, and lysis buffer was added to adjust the protein concentration of the supernatant to 5 mg/mL. A total of 10 uL supernatant then was mixed with 50 uL blank solution or reaction solution (provided in the kit) in a 96-well plate and incubated at $37°C$ for 1 hour. A total of 50 μL of 3% fresh-made acetic acid solution subsequently was added to each well to stop the reaction, and the absorbance was measured at 492 nm for the calculation of formazan production (mol). FAO activity was presented as INT-formazan (mol) per gram of protein.

LysoPLD Activity Assay

LysoPLD activity was measured as previously described.[80] Briefly, 10 μL mouse serum or rmATX (2 ug/mL in phosphate-buffered saline) was incubated with 2 mmol/L 1-myristoyl (14:0)– lysophosphatidylcholine (Avanti Polar Lipids, Inc, Alabaster, AL) in 90 μL assay buffer (100 mmol/L Tris–HCl, pH 9.0, 500 mmol/L NaCl, 5 mmol/L $MgCl_2$, 5 mmol/L $CaCl_2$, and 0.05% Triton X-100) for 4 hours at $37°C$ to allow for autotaxin-mediated choline release. Subsequently, 100 μL reaction buffer containing 4.5 mmol/L 4-aminoantioyrine, 2.7 mmol/L TOOS reagent (N-ethyl-N-[2-hydroxy-3-sulfopropyl]-3-methylaniline, a hydrogen donor), 20 U/mL horseradish peroxidase, 3 U/mL choline oxidase, 4.5 mmol/L $MgCl_2$, 100 mmol/L Tris, pH 8.0) was added and incubated for another 10 minutes at room temperature to allow for color reaction. The absorbance was measured at 555 nm for the calculation of choline production (nmol) per microliter of serum per hour (for serum), or choline production (μmol) per milligram of protein per minute (for rmATX).

Production, Purification, and Validation of Anti-Autotaxin Neutralizing Antibody

rmATX (42771; Immunodiagnostics, Ltd) was used as antigen for 4 consecutive immunizations of New Zealand

white rabbits for 2 months. After the antibody titer in the serum reached more than 10^{-6}, blood samples were taken from marginal ear veins of sedated rabbits, followed by sequential affinity purification of anti-autotaxin IgG with protein G–agarose and rmATX-conjugated sepharose 4b resin. Nonimmune rabbit IgG purified from preimmune rabbit serum was used as control. The neutralizing activity of anti-autotaxin IgG was validated by its ability to block the activity of rmATX in vitro and to inhibit rmATX-induced Erk activation in HepG2 cells (ATCC, Manassas, VA) maintained in DMEM (Gibco, Carlsbad, CA).

Cell Culture and Luciferase Reporter Assay

Huh7 cell lines obtained from the Cell Bank of Type Culture Collection at the Chinese Academy of Sciences were maintained in DMEM (Gibco) supplemented with 10% FBS (Gibco), 100 IU/mL penicillin, and 100 μg/mL streptomycin. To evaluate the effects of the ATX–LPA axis on FGF21 expression and secretion, cells grown in DMEM were treated with rhATX (41771; Immunodiagnostics, Ltd, Hong Kong, China), lysophosphatidic acid (62215; Cayman, Ann Arbor, MI), fenofibrate (Abbott Laboratories, Chicago, IL), U0126 (9903; Cell Signaling Technology), wortmannin (W1628; Sigma), PF8380 (12018; Cayman), and Ki16425 (10012659; Cayman) at the concentration specified in each figure legend. For luciferase reporter assay, Huh7 cells were seeded in 24-well plates and were transfected with 0.5 μg PPAR response element X3-TK-luc plasmid (plasmid 1015; Addgene) and 0.5 μg HSV-thymidine kinase Renilla luciferase reporter plasmid (pRL-TK) per well with

Table 3. Primers Used for Real-Time PCR

Gene name	Kind	Primer sequences, 5'-3'	Gene name	Kind	Primer sequences, 5'-3'
Murine	Forward	CATTTATTGGTGGAACGCAGA	Murine	Forward	GCATCCACGAAACCACCTA
Enpp2	Reverse	CTACAAAAACAGTCTGCATGC	Acta2	Reverse	CACGAGTAACAAATCAAAGC
Murine	Forward	CTGGGGGTCTACCAAGCATA	Murine	Forward	GACTGCGAGGAGGACCAAAA
Fgf21	Reverse	CACCCAGGATTTGAATGACC	Fgf15	Reverse	CAGCCCGTATATCTTGCCGT
Murine	Forward	ACCTTCTACAATGAGCTGCG	Murine	Forward	CCAGTGTCATTCCACCAGA
β-actin	Reverse	CTGGATGGCTACGTACATGG	Fetuin-A	Reverse	CGCAGCTATCACAAACTCCA
Murine	Forward	TAACTTCCTCACTCGAAGCCA	Murine	Forward	AGCACCAAGAACTACTCCCC
Acox-1	Reverse	AGTTCCATGACCCATCTCTGTC	Angptl3	Reverse	ATAAACGGCAGAGCAGTCGG
Murine	Forward	CAGAGGATGGACACTGTAAAGG	Murine	Forward	AGCTCATTGGCTTGACTCCC
Cpt-1α	Reverse	CGGCACTTCTTGATCAAGCC	Angptl4	Reverse	GAAGTCCACAGAGCCGTTCA
Murine	Forward	CTTGCTTGGCATCAACATCGCAGA	Murine	Forward	ACTACGACAGCTTCTCCTTG
Lcad	Reverse	ATTGGAGTACGCTTGCTCTTCCCA	Angptl6	Reverse	AGTGCTGAAAGGTTTGTCAT
Murine	Forward	ACCAAAGCTTGGATCACCAACTCC	Murine	Forward	AGGCTCTGTGTGGATGGACT
Scad	Reverse	AACCAGGAAGGCACTGATACCCTT	Fgl1	Reverse	CCAACCTTCCCTTCCCATCA
Murine	Forward	GGATGACGGAGCCAATG	Murine	Forward	GAGGCCCCTTATCATTCCGC
Mcad	Reverse	GGGTGTCGGCTTCCACAATG	Dpp4	Reverse	ACCCCACTGTTGTTAGGATGG
Murine	Forward	TGCTATCGGGGTGTTAATGA	Murine	Forward	GGCCAGTTCACTCTGGGAAA
Scd-1	Reverse	TCTTGTGGCATGGTTAATCCTA	Lcn2	Reverse	TGGCGAACTGGTTGTAGTCC
Murine	Forward	GGAGGTGGTGATAGCCGGTAT	Murine	Forward	CCTCTAATGGCGTGGTCTCG
Fasn	Reverse	TGGGTAATCCATAGAGCCCAG	Apelin	Reverse	GTCTCCAAGGGCAGTCCAAA
Murine	Forward	AGATGACGTGGCAAAGAACAG	Murine	Forward	CTATGCCACCTTGGTCACCT
Cd36	Reverse	CCTTGGCTAGATAACGAACTCTG	Leptin	Reverse	ACCAAACCAAGCATTTTTGC
Murine	Forward	CCAATCGACTCACGGGTTCA	Murine	Forward	AAGTGGGAGTGGGCTTTGC
Ldlr	Reverse	ACAGTGTCGACTTCTCTAGGC	Fabp4	Reverse	TGGTGACCAAATCCCCATTT
Murine	Forward	GTCCCCAAAGGGATGAGAAGT	Murine	Forward	GGAGAGAAAGGAGATGCAGGT
Tnf-α	Reverse	GCTCCTCCACTTGGTGGTTT	Adipoq	Reverse	CTTTCCTGCCAGGGGTTC
Murine	Forward	GCAACTGTTCCTGAACTCAACT	human	Forward	ATGCCTGAATGACTCCACTGTT
Il1b	Reverse	ATCTTTTGGGGTCCGTCAACT	ENPP2	Reverse	AGGACTAAATGTGGCAACTGTG
Murine	Forward	TTTCTAGCCACACCAGGCAGATGA	human	Forward	ATCGCTCCACTTTGACCCTG
Timp1	Reverse	GGTTTGCTGGGAAGGCATTTGAGT	FGF21	Reverse	GGGCTTCGGACTGGTAAACA
Murine	Forward	TTCCCTTCCTTTCTCGCCAC	human	Forward	GTCTTCCCCTCCATCGTG
Enpp2-shRNA	Reverse	AGCCCGAGATAGGGTTGAGT	Beta-actin	Reverse	GTACTTCAGGGTGAGGATGC
Murine	Forward	GAAACCCGAGGTATGCTTGA	human	Forward	CCGGAGAGATTCGGAGATGC
Col1a1	Reverse	GACCAGGAGGACCAGGAAGT	VLCAD	Reverse	TCAGAGGGGTGGGAATCTGA
Murine	Forward	CGAGGTGACAGAGACCACAA	human	Forward	AGAAGCTGTCACCACAGTAGC
Fibronectin	Reverse	CTGGAGTCAAGCCAGACACA	PPARa	Reverse	TGAAAGCGTGTCCGTGATGA

polyethylenimine (PEI). At 48 hours after transfection, cells were treated further with LPA (10 μmol/L), U0126 (10 μmol/L), and wortmannin (2 μmol/L) in the presence or absence of fenofibrate (50 μmol/L) for 24 hours, and then were collected for analysis of firefly luciferase/Renilla luciferase activity using the Dual-Luciferase Reporter Assay System (E1960; Promega).

Generation and Titration of AAVs

The shRNA targeting autotaxin (target sequence: CCTGTACCAAATCTGACATAT) and control shRNA with scrambled sequence (CCTAAGGTTAAGTCGCCCTCG) in pAAV-EGFP-U6 vectors were purchased from VectorBuilder (Santa Clara, CA). The sequence targeting the 3' untranslated region of autotaxin mRNA was chosen from the database provided by VectorBuilder, based on the predicted high knockdown efficiency. In vitro validation for the knockdown efficiency of shRNA was conducted by transfection of shRNA targeting autotaxin or control shRNA into Hepa1–6 cells (ATCC, Manassas, VA) cultured in DMEM (supplemented with 10% FBS, 100 IU/mL penicillin, and 100 ug/mL streptomycin) and examination of the mRNA level of autotaxin at 4 days after transfection.

To generate AAV, 500 μL DMEM was mixed with 120 μL of 1 mg/mL PEI to generate solution A, while another 500 μL DMEM was mixed with 12 μg of shRNA plasmid, 10 μg pXX6, and 10 μg p5E18-VD2/8 to make solution B. After mixing solutions A and B vigorously, the PEI–DNA complex was incubated at room temperature for 20 minutes and added into the 150-mm culture dish of HEK293T cells (ATCC). Six hours after transfection, the medium was replaced with fresh complete DMEM medium. The medium of HEK293T cells was harvested 3 days after transfection. The concentration and purification of AAV were conducted following the standard protocol of AAVanced Concentration Reagent (AAV110A-1; System Biosciences, Inc, Palo Alto, CA). For the titration of AAV, 5 μL concentrated AAV was added with buffer AL (19075; QIAGEN, Inc, Santa Clarita, CA) and incubated at 55°C for 30 minutes. The mix then was proceeded to Zymoclean Gel DNA Recovery Kit (Zymo Research Corporation, Irvine, CA). Eluted DNA was used as the amplification template for the titration of AAV by real-time PCR, and serially diluted shRNA plasmids were used to generate a standard curve showing the correlation between the cycle threshold (CT) value and the copy number of vector genome.

Statistics

For animal studies, data statistical analyses were performed using GraphPad Prism 6 (GraphPad Software, Inc La Jolla, CA). The results are expressed as means ± SEM. Animal sample size (N number) for each experiment was chosen according to previous reports of similar types of experiments. For comparison between 2 groups, statistical significance was determined by the 2-tailed Student t test. For multiple comparisons within more than 2 groups, statistical calculations were performed by 1-way analysis of variance followed by Tukey multiple comparisons using Prism 6. $P < .05$ was considered statistically significant. For the clinical study, statistical analyses were performed with SPSS software (version 26.0; SPSS, Inc, Chicago, IL) and GraphPad Prism 6. Data are presented as means ± SEM. P values were assessed by the Mann–Whitney U test or the Kruskal–Wallis test with the Dunn multiple comparison test among groups for continuous parameters and by the chi-squared test for categoric parameters. Multiple regression was used to assess associations and adjust for conventional confounders such as age, sex, and BMI for correlation coefficient. $P < .05$ was considered statistically significant.

All authors had access to the study data and reviewed and approved the final manuscript.

References

1. Fan JG, Kim SU, Wong VW. New trends on obesity and NAFLD in Asia. J Hepatol 2017;67:862–873.
2. Younossi Z, Anstee QM, Marietti M, Hardy T, Henry L, Eslam M, George J, Bugianesi E. Global burden of NAFLD and NASH: trends, predictions, risk factors and prevention. Nat Rev Gastroenterol Hepatol 2018;15:11–20.
3. Attia SL, Softic S, Mouzaki M. Evolving role for pharmacotherapy in NAFLD/NASH. Clin Transl Sci 2021; 14:11–19.
4. Friedman SL, Neuschwander-Tetri BA, Rinella M, Sanyal AJ. Mechanisms of NAFLD development and therapeutic strategies. Nat Med 2018;24:908–922.
5. Eslam M, Sanyal AJ, George J. MAFLD: a consensus-driven proposed nomenclature for metabolic associated fatty liver disease. Gastroenterology 2020; 158:1999–2014.e1.
6. Kucukoglu O, Sowa JP, Mazzolini GD, Syn WK, Canbay A. Hepatokines and adipokines in NASH-related hepatocellular carcinoma. J Hepatol 2021;74:442–457.
7. Polyzos SA, Kountouras J, Mantzoros CS. Adipokines in nonalcoholic fatty liver disease. Metabolism 2016; 65:1062–1079.
8. Geng L, Lam KSL, Xu A. The therapeutic potential of FGF21 in metabolic diseases: from bench to clinic. Nat Rev Endocrinol 2020;16:654–667.
9. Ferry G, Tellier E, Try A, Gres S, Naime I, Simon MF, Rodriguez M, Boucher J, Tack I, Gesta S, Chomarat P, Dieu M, Raes M, Galizzi JP, Valet P, Boutin JA, Saulnier-Blache JS. Autotaxin is released from adipocytes, catalyzes lysophosphatidic acid synthesis, and activates preadipocyte proliferation. Up-regulated expression with adipocyte differentiation and obesity. J Biol Chem 2003; 278:18162–18169.
10. Rancoule C, Dusaulcy R, Treguer K, Gres S, Attane C, Saulnier-Blache JS. Involvement of autotaxin/lysophosphatidic acid signaling in obesity and impaired glucose homeostasis. Biochimie 2014;96:140–143.
11. Yuelling LM, Fuss B. Autotaxin (ATX): a multi-functional and multi-modular protein possessing enzymatic lysoPLD activity and matricellular properties. Biochim Biophys Acta 2008;1781:525–530.
12. Yung YC, Stoddard NC, Chun J. LPA receptor signaling: pharmacology, physiology, and pathophysiology. J Lipid Res 2014;55:1192–1214.

13. Kihara Y, Mizuno H, Chun J. Lysophospholipid receptors in drug discovery. Exp Cell Res 2015;333:171–177.

14. Wunsch E, Krawczyk M, Milkiewicz M, Trottier J, Barbier O, Neurath MF, Lammert F, Kremer AE, Milkiewicz P. Serum autotaxin is a marker of the severity of liver injury and overall survival in patients with cholestatic liver diseases. Sci Rep 2016;6:30847.

15. Bain G, Shannon KE, Huang F, Darlington J, Goulet L, Prodanovich P, Ma GL, Santini AM, Stein AJ, Lonergan D, King CD, Calderon I, Lai A, Hutchinson JH, Evans JF. Selective inhibition of autotaxin is efficacious in mouse models of liver fibrosis. J Pharmacol Exp Ther 2017;360:1–13.

16. Kaffe E, Katsifa A, Xylourgidis N, Ninou I, Zannikou M, Harokopos V, Foka P, Dimitriadis A, Evangelou K, Moulas AN, Georgopoulou U, Gorgoulis VG, Dalekos GN, Aidinis V. Hepatocyte autotaxin expression promotes liver fibrosis and cancer. Hepatology 2017; 65:1369–1383.

17. Brandon JA, Kraemer M, Vandra J, Halder S, Ubele M, Morris AJ, Smyth SS. Adipose-derived autotaxin regulates inflammation and steatosis associated with diet-induced obesity. PLoS One 2019;14:e0208099.

18. Nishimura S, Nagasaki M, Okudaira S, Aoki J, Ohmori T, Ohkawa R, Nakamura K, Igarashi K, Yamashita H, Eto K, Uno K, Hayashi N, Kadowaki T, Komuro I, Yatomi Y, Nagai R. ENPP2 contributes to adipose tissue expansion and insulin resistance in diet-induced obesity. Diabetes 2014;63:4154–4164.

19. Federico L, Ren H, Mueller PA, Wu T, Liu S, Popovic J, Blalock EM, Sunkara M, Ovaa H, Albers HM, Mills GB, Morris AJ, Smyth SS. Autotaxin and its product lysophosphatidic acid suppress brown adipose differentiation and promote diet-induced obesity in mice. Mol Endocrinol 2012;26:786–797.

20. Dusaulcy R, Rancoule C, Gres S, Wanecq E, Colom A, Guigne C, van Meeteren LA, Moolenaar WH, Valet P, Saulnier-Blache JS. Adipose-specific disruption of autotaxin enhances nutritional fattening and reduces plasma lysophosphatidic acid. J Lipid Res 2011; 52:1247–1255.

21. Reeves VL, Trybula JS, Wills RC, Goodpaster BH, Dube JJ, Kienesberger PC, Kershaw EE. Serum autotaxin/ENPP2 correlates with insulin resistance in older humans with obesity. Obesity 2015;23:2371–2376.

22. Watanabe N, Nakamura K, Ohkawa R, Tomiya T, Yanase M, Tejima K, Nishikawa T, Omata M, Fujiwara K, Yatomi Y, Ikeda H. Autotaxin and lysophosphatidic acid in the blood in patients of viral hepatitis. J Clin Virol 2006; 36, S171-S.

23. Watanabe N, Ikeda H, Nakamura K, Ohkawa R, Kume Y, Aoki J, Hama K, Okudaira S, Tanaka M, Tomiya T, Yanase M, Tejima K, Nishikawa T, Arai M, Arai H, Omata M, Fujiwara K, Yatomi Y. Both plasma lysophosphatidic acid and serum autotaxin levels are increased in chronic hepatitis C. J Clin Gastroenterol 2007;41:616–623.

24. Kondo M, Ishizawa T, Enooku K, Tokuhara Y, Ohkawa R, Uranbileg B, Nakagawa H, Tateishi R, Yoshida H, Kokudo N, Koike K, Yatomi Y, Ikeda H. Increased serum autotaxin levels in hepatocellular carcinoma patients were caused by background liver fibrosis but not by carcinoma. Clin Chim Acta 2014;433:128–134.

25. Ikeda H, Kobayashi M, Kumada H, Enooku K, Koike K, Kurano M, Sato M, Nojiri T, Kobayashi T, Ohkawa R, Shimamoto S, Igarashi K, Aoki J, Yatomi Y. Performance of autotaxin as a serum marker for liver fibrosis. Ann Clin Biochem 2018;55:469–477.

26. She S, Yang M, Hu H, Hu P, Yang Y, Ren H. Proteomics based identification of autotaxin as an anti-hepatitis B virus factor and a promoter of hepatoma cell invasion and migration. Cell Physiol Biochem 2018;45:744–760.

27. Rachakonda VP, Reeves VL, Aljammal J, Wills RC, Trybula JS, DeLany JP, Kienesberger PC, Kershaw EE. Serum autotaxin is independently associated with hepatic steatosis in women with severe obesity. Obesity 2015;23:965–972.

28. Nascimbeni F, Bedossa P, Fedchuk L, Pais R, Charlotte F, Lebray P, Poynard T, Ratziu V. Clinical validation of the FLIP algorithm and the SAF score in patients with non-alcoholic fatty liver disease. J Hepatol 2020;72:828–838.

29. Rancoule C, Dusaulcy R, Treguer K, Gres S, Guigne C, Quilliot D, Valet P, Saulnier-Blache JS. Depot-specific regulation of autotaxin with obesity in human adipose tissue. J Physiol Biochem 2012;68:635–644.

30. Li X, Cheng KK, Liu Z, Yang JK, Wang B, Jiang X, Zhou Y, Hallenborg P, Hoo RL, Lam KS, Ikeda Y, Gao X, Xu A. The MDM2-p53-pyruvate carboxylase signalling axis couples mitochondrial metabolism to glucose-stimulated insulin secretion in pancreatic beta-cells. Nat Commun 2016;7:11740.

31. Liu Z, Jin L, Yang JK, Wang B, Wu KKL, Hallenborg P, Xu A, Cheng KKY. The dysfunctional MDM2-p53 axis in adipocytes contributes to aging-related metabolic complications by induction of lipodystrophy. Diabetes 2018; 67:2397–2409.

32. Katsifa A, Kaffe E, Nikolaidou-Katsaridou N, Economides AN, Newbigging S, McKerlie C, Aidinis V. The bulk of autotaxin activity is dispensable for adult mouse life. PLoS One 2015;10:e0143083.

33. Lin Z, Pan X, Wu F, Ye D, Zhang Y, Wang Y, Jin L, Lian Q, Huang Y, Ding H, Triggle C, Wang K, Li X, Xu A. Fibroblast growth factor 21 prevents atherosclerosis by suppression of hepatic sterol regulatory element-binding protein-2 and induction of adiponectin in mice. Circulation 2015;131:1861–1871.

34. Gierse J, Thorarensen A, Beltey K, Bradshaw-Pierce E, Cortes-Burgos L, Hall T, Johnston A, Murphy M, Nemirovskiy O, Ogawa S, Pegg L, Pelc M, Prinsen M, Schnute M, Wendling J, Wene S, Weinberg R, Wittwer A, Zweifel B, Masferrer J. A novel autotaxin inhibitor reduces lysophosphatidic acid levels in plasma and the site of inflammation. J Pharmacol Exp Ther 2010; 334:310–317.

35. Ohta H, Sato K, Murata N, Damirin A, Malchinkhuu E, Kon J, Kimura T, Tobo M, Yamazaki Y, Watanabe T, Yagi M, Sato M, Suzuki R, Murooka H, Sakai T, Nishitoba T, Im DS, Nochi H, Tamoto K, Tomura H, Okajima F. Ki16425, a subtype-selective antagonist for

EDG-family lysophosphatidic acid receptors. Mol Pharmacol 2003;64:994–1005.

36. Geraldo LHM, Spohr T, Amaral RFD, Fonseca A, Garcia C, Mendes FA, Freitas C, dosSantos MF, Lima FRS. Role of lysophosphatidic acid and its receptors in health and disease: novel therapeutic strategies. Signal Transduct Target Ther 2021;6:45.

37. Han L, Shen WJ, Bittner S, Kraemer FB, Azhar S. PPARs: regulators of metabolism and as therapeutic targets in cardiovascular disease. Part I: PPAR-α. Future Cardiol 2017;13:259–278.

38. Gross B, Pawlak M, Lefebvre P, Staels B. PPARs in obesity-induced T2DM, dyslipidaemia and NAFLD. Nat Rev Endocrinol 2017;13:36–49.

39. Kim JB, Wright HM, Wright M, Spiegelman BM. ADD1/SREBP1 activates PPARgamma through the production of endogenous ligand. Proc Natl Acad Sci U S A 1998; 95:4333–4337.

40. Agassandian M, Miakotina OL, Andrews M, Mathur SN, Mallampalli RK. Pseudomonas aeruginosa and sPLA2 IB stimulate ABCA1-mediated phospholipid efflux via ERK-activation of PPARalpha-RXR. Biochem J 2007; 403:409–420.

41. Juge-Aubry CE, Hammar E, Siegrist-Kaiser C, Pernin A, Takeshita A, Chin WW, Burger AG, Meier CA. Regulation of the transcriptional activity of the peroxisome proliferator-activated receptor alpha by phosphorylation of a ligand-independent trans-activating domain. J Biol Chem 1999;274:10505–10510.

42. Barger PM, Brandt JM, Leone TC, Weinheimer CJ, Kelly DP. Deactivation of peroxisome proliferator-activated receptor-alpha during cardiac hypertrophic growth. J Clin Invest 2000;105:1723–1730.

43. Zarei M, Pizarro-Delgado J, Barroso E, Palomer X, Vázquez-Carrera M. Targeting FGF21 for the treatment of nonalcoholic steatohepatitis. Trends Pharmacol Sci 2020;41:199–208.

44. Ye D, Wang Y, Li H, Jia W, Man K, Lo CM, Wang Y, Lam KS, Xu A. Fibroblast growth factor 21 protects against acetaminophen-induced hepatotoxicity by potentiating peroxisome proliferator-activated receptor coactivator protein-1alpha-mediated antioxidant capacity in mice. Hepatology 2014;60:977–989.

45. Geng L, Liao B, Jin L, Huang Z, Triggle CR, Ding H, Zhang J, Huang Y, Lin Z, Xu A. Exercise alleviates obesity-induced metabolic dysfunction via enhancing FGF21 sensitivity in adipose tissues. Cell Rep 2019; 26:2738–2752, e4.

46. Talukdar S, Kharitonenkov A. FGF19 and FGF21: in NASH we trust. Mol Metab 2021;46:101152.

47. Liu L, Liu C, Zhao M, Zhang Q, Lu Y, Liu P, Yang H, Yang J, Chen X, Yao Y. The pharmacodynamic and differential gene expression analysis of PPAR α/δ agonist GFT505 in CDAHFD-induced NASH model. PLoS One 2020;15:e0243911.

48. Sugasawa T, Ono S, Yonamine M, Fujita SI, Matsumoto Y, Aoki K, Nakano T, Tamai S, Yoshida Y, Kawakami Y, Takekoshi K. One week of CDAHFD induces steatohepatitis and mitochondrial dysfunction with oxidative stress in liver. Int J Mol Sci 2021; 22:5851.

49. D'Souza K, Paramel GV, Kienesberger PC. Lysophosphatidic acid signaling in obesity and insulin resistance. Nutrients 2018;10:399.

50. Valdes-Rives SA, Gonzalez-Arenas A. Autotaxin-lysophosphatidic acid: from inflammation to cancer development. Mediators Inflamm 2017;2017:9173090.

51. Federico L, Jeong KJ, Vellano CP, Mills GB. Autotaxin, a lysophospholipase D with pleomorphic effects in oncogenesis and cancer progression. J Lipid Res 2016; 57:25–35.

52. Tezze C, Romanello V, Sandri M. FGF21 as modulator of metabolism in health and disease. Front Physiol 2019; 10:419.

53. Maratos-Flier E. Fatty liver and FGF21 physiology. Exp Cell Res 2017;360:2–5.

54. Fisher FM, Chui PC, Nasser IA, Popov Y, Cunniff JC, Lundasen T, Kharitonenkov A, Schuppan D, Flier JS, Maratos-Flier E. Fibroblast growth factor 21 limits lipotoxicity by promoting hepatic fatty acid activation in mice on methionine and choline-deficient diets. Gastroenterology 2014;147:1073–1083.e6.

55. Yu Y, He J, Li S, Song L, Guo X, Yao W, Zou D, Gao X, Liu Y, Bai F, Ren G, Li D. Fibroblast growth factor 21 (FGF21) inhibits macrophage-mediated inflammation by activating Nrf2 and suppressing the NF-κB signaling pathway. Int Immunopharmacol 2016;38:144–152.

56. Xu P, Zhang Y, Liu Y, Yuan Q, Song L, Liu M, Liu Z, Yang Y, Li J, Li D, Ren G. Fibroblast growth factor 21 attenuates hepatic fibrogenesis through TGF-β/smad2/3 and NF-κB signaling pathways. Toxicol Appl Pharmacol 2016;290:43–53.

57. Ritchie M, Hanouneh IA, Noureddin M, Rolph T, Alkhouri N. Fibroblast growth factor (FGF)-21 based therapies: a magic bullet for nonalcoholic fatty liver disease (NAFLD)? Expert Opin Investig Drugs 2020;29:197–204.

58. Tillman EJ, Rolph T. FGF21: an emerging therapeutic target for non-alcoholic steatohepatitis and related metabolic diseases. Front Endocrinol (Lausanne) 2020; 11:601290.

59. Harrison SA, Ruane PJ, Freilich BL, Neff G, Patil R, Behling CA, Hu C, Fong E, de Temple B, Tillman EJ, Rolph TP, Cheng A, Yale K. Efruxifermin in non-alcoholic steatohepatitis: a randomized, double-blind, placebo-controlled, phase 2a trial. Nat Med 2021;27:1262–1271.

60. Rader DJ, Maratos-Flier E, Nguyen A, Hom D, Ferriere M, Li Y, Kompa J, Martic M, Hinder M, Basson CT, Yowe D, Diener J, Goldfine AB. LLF580, an FGF21 analog, reduces triglycerides and hepatic fat in obese adults with modest hypertriglyceridemia. J Clin Endocrinol Metab 2022;107:e57–e70.

61. Botta M, Audano M, Sahebkar A, Sirtori CR, Mitro N, Ruscica M. PPAR agonists and metabolic syndrome: an established role? Int J Mol Sci 2018;19:1197.

62. Lundåsen T, Hunt MC, Nilsson LM, Sanyal S, Angelin B, Alexson SE, Rudling M. PPARalpha is a key regulator of hepatic FGF21. Biochem Biophys Res Commun 2007; 360:437–440.

63. Pawlak M, Lefebvre P, Staels B. Molecular mechanism of PPARalpha action and its impact on lipid metabolism, inflammation and fibrosis in non-alcoholic fatty liver disease. J Hepatol 2015;62:720–733.

64. Wang Y, Nakajima T, Gonzalez FJ, Tanaka N. PPARs as metabolic regulators in the liver: lessons from liver-specific PPAR-null mice. Int J Mol Sci 2020;21:2061.

65. Montagner A, Polizzi A, Fouché E, Ducheix S, Lippi Y, Lasserre F, Barquissau V, Régnier M, Lukowicz C, Benhamed F, Iroz A, Bertrand-Michel J, Al Saati T, Cano P, Mselli-Lakhal L, Mithieux G, Rajas F, Lagarrigue S, Pineau T, Loiseau N, Postic C, Langin D, Wahli W, Guillou H. Liver PPARα is crucial for whole-body fatty acid homeostasis and is protective against NAFLD. Gut 2016;65:1202–1214.

66. Seo YS, Kim JH, Jo NY, Choi KM, Baik SH, Park JJ, Kim JS, Byun KS, Bak YT, Lee CH, Kim A, Yeon JE. PPAR agonists treatment is effective in a nonalcoholic fatty liver disease animal model by modulating fatty-acid metabolic enzymes. J Gastroenterol Hepatol 2008;23:102–109.

67. Nakajima T, Yang Y, Lu Y, Kamijo Y, Yamada Y, Nakamura K, Koyama M, Yamaguchi S, Sugiyama E, Tanaka N, Aoyama T. Decreased fatty acid β-oxidation is the main cause of fatty liver induced by polyunsaturated fatty acid deficiency in mice. Tohoku J Exp Med 2017; 242:229–239.

68. Fernández-Miranda C, Pérez-Carreras M, Colina F, López-Alonso G, Vargas C, Solís-Herruzo JA. A pilot trial of fenofibrate for the treatment of non-alcoholic fatty liver disease. Dig Liver Dis 2008;40:200–205.

69. Benesch MGK, Ko YM, McMullen TPW, Brindley DN. Autotaxin in the crosshairs: taking aim at cancer and other inflammatory conditions. FEBS Lett 2014; 588:2712–2727.

70. Song J, Clair T, Noh JH, Eun JW, Ryu SY, Lee SN, Ahn YM, Kim SY, Lee SH, Park WS, Yoo NJ, Lee JY, Nam SW. Autotaxin (lysoPLD/NPP2) protects fibroblasts from apoptosis through its enzymatic product, lyso-phosphatidic acid, utilizing albumin-bound substrate. Biochem Biophys Res Commun 2005;337:967–975.

71. Tang X, Wuest M, Benesch MGK, Dufour J, Zhao Y, Curtis JM, Monjardet A, Heckmann B, Murray D, Wuest F, Brindley DN. Inhibition of autotaxin with GLPG1690 increases the efficacy of radiotherapy and chemotherapy in a mouse model of breast cancer. Mol Cancer Ther 2020;19:63–74.

72. Jia Y, Li Y, Xu XD, Tian Y, Shang H. Design and development of autotaxin inhibitors. Pharmaceuticals (Basel) 2021;14:1203.

73. Pappachan JM, Babu S, Krishnan B, Ravindran NC. Non-alcoholic fatty liver disease: a clinical update. J Clin Transl Hepatol 2017;5:384–393.

74. Hotta Y, Nakamura H, Konishi M, Murata Y, Takagi H, Matsumura S, Inoue K, Fushiki T, Itoh N. Fibroblast growth factor 21 regulates lipolysis in white adipose tissue but is not required for ketogenesis and triglyceride clearance in liver. Endocrinology 2009;150:4625–4633.

75. Wu X, Shu L, Zhang Z, Li J, Zong J, Cheong LY, Ye D, Lam KSL, Song E, Wang C, Xu A, Hoo RLC. Adipocyte fatty acid binding protein promotes the onset and progression of liver fibrosis via mediating the crosstalk between liver sinusoidal endothelial cells and hepatic stellate cells. Adv Sci (Weinh) 2021;8:e2003721.

76. Claude A. Fractionation of mammalian liver cells by differential centrifugation: II. Experimental procedures and results. J Exp Med 1946;84:61–89.

77. Mopuri R, Kalyesubula M, Rosov A, Edery N, Moallem U, Dvir H. Improved Folch method for liver-fat quantification. Front Vet Sci 2020;7:594853.

78. Cheng X, Geng F, Pan M, Wu X, Zhong Y, Wang C, Tian Z, Cheng C, Zhang R, Puduvalli V, Horbinski C, Mo X, Han X, Chakravarti A, Guo D. Targeting DGAT1 ameliorates glioblastoma by increasing fat catabolism and oxidative stress. Cell Metab 2020;32:229–242.e8.

79. Kwong SC, Jamil AHA, Rhodes A, Taib NA, Chung I. Metabolic role of fatty acid binding protein 7 in mediating triple-negative breast cancer cell death via PPAR-α signaling. J Lipid Res 2019;60:1807–1817.

80. Morris AJ, Smyth SS. Measurement of autotaxin/lyso-phospholipase D activity. Methods Enzymol 2007; 434:89–104.

Correspondence

Address correspondence to: Aimin Xu, PhD, Department of Medicine, The University of Hong Kong, L8-40, 21 Sassoon Road, Pokfulam, Hong Kong. Fax: +852-28162095. e-mail: amxu@hku.hk; or Yong Wang, MD, Department of General Surgery, The Second Teaching Hospital of Anhui Medical University, NO. 678 Furong Road, Economic and Technological Development Zone, Hefei, China. e-mail: wangyong@ahmu.edu.cn; Tel: +86-0551-63869559.